nature metabolism

Article

https://doi.org/10.1038/s42255-024-01177-7

Intestinal TM6SF2 protects against metabolic dysfunction-associated steatohepatitis through the gut–liver axis

Received: 18 September 2023

Accepted: 14 November 2024

Published online: 8 January 2025

Check for updates

Xiang Zhang[1], Harry Cheuk-Hay Lau[1], Suki Ha[1], Chuanfa Liu[1], Cong Liang[2], Hye Won Lee[3], Queena Wing-Yin Ng[1], Yi Zhao[1,2], Fenfen Ji[1], Yunfei Zhou[1], Yasi Pan[1], Yang Song[1,4], Yating Zhang[1], Jennie Ching Yin Lo[1], Alvin Ho Kwan Cheung[5], Jianfeng Wu[6], Xiaoxing Li[2], Hongzhi Xu[4], Chi Chun Wong[1], Vincent Wai-Sun Wong[1] ✉ & Jun Yu[1] ✉

Transmembrane-6 superfamily member 2 (TM6SF2) regulates hepatic fat metabolism and is associated with metabolic dysfunction-associated steatohepatitis (MASH). *TM6SF2* genetic variants are associated with steatotic liver disease. The pathogenesis of MASH involves genetic factors and gut microbiota alteration, yet the role of host–microbe interactions in MASH development remains unclear. Here, we discover that mice with intestinal epithelial cell-specific knockout of *Tm6sf2* (*Tm6sf2*$^{\Delta IEC}$) develop MASH, accompanied by impaired intestinal barrier and microbial dysbiosis. Transplanting stools from *Tm6sf2*$^{\Delta IEC}$ mice induces steatohepatitis in germ-free recipient mice, whereas MASH is alleviated in *Tm6sf2*$^{\Delta IEC}$ mice co-housed with wild-type mice. Mechanistically, *Tm6sf2*-deficient intestinal cells secrete more free fatty acids by interacting with fatty acid-binding protein 5 to induce intestinal barrier dysfunction, enrichment of pathobionts, and elevation of lysophosphatidic acid (LPA) levels. LPA is translocated from the gut to the liver, contributing to lipid accumulation and inflammation. Pharmacological inhibition of the LPA receptor suppresses MASH in both *Tm6sf2*$^{\Delta IEC}$ and wild-type mice. Hence, modulating microbiota or blocking the LPA receptor is a potential therapeutic strategy in TM6SF2 deficiency-induced MASH.

Metabolic dysfunction-associated steatotic liver disease (MASLD) is the leading chronic liver disease worldwide, affecting one billion individuals globally[1], while 23% of individuals with MASLD could progress to its more severe subtype—MASH—in 3 years[2]. MASH is a complex and progressive disease, and genetic factors are important in shaping the susceptibility and progression of MASH[3]. An exome-wide association study identified a *Tm6sf2* loss-of-function variant (missense mutation, encoding p.Glu167Lys) as an independent risk factor of hepatic steatosis[4]. TM6SF2 is predominantly expressed in human liver and small intestine[4], and it is a regulator of liver fat metabolism, influencing triglyceride secretion and lipid droplet content[5]. Using liver-specific transgenic mice, the functional role of hepatic TM6SF2 in mediating intracellular cholesterol homeostasis has been revealed[6]. On the other hand, liver-specific *Tm6sf2* deletion could impair hepatic secretion of very low-density lipoprotein cholesterol, thereby causing lipid accumulation in the liver and accelerating MASLD progression[7]. However, although the expression of TM6SF2 in the small intestine is even higher than the liver[8], and *TM6SF2* variant is associated with

A full list of affiliations appears at the end of the paper. ✉e-mail: wongv@cuhk.edu.hk; junyu@cuhk.edu.hk

https://doi.org/10.1038/s42255-024-01177-7

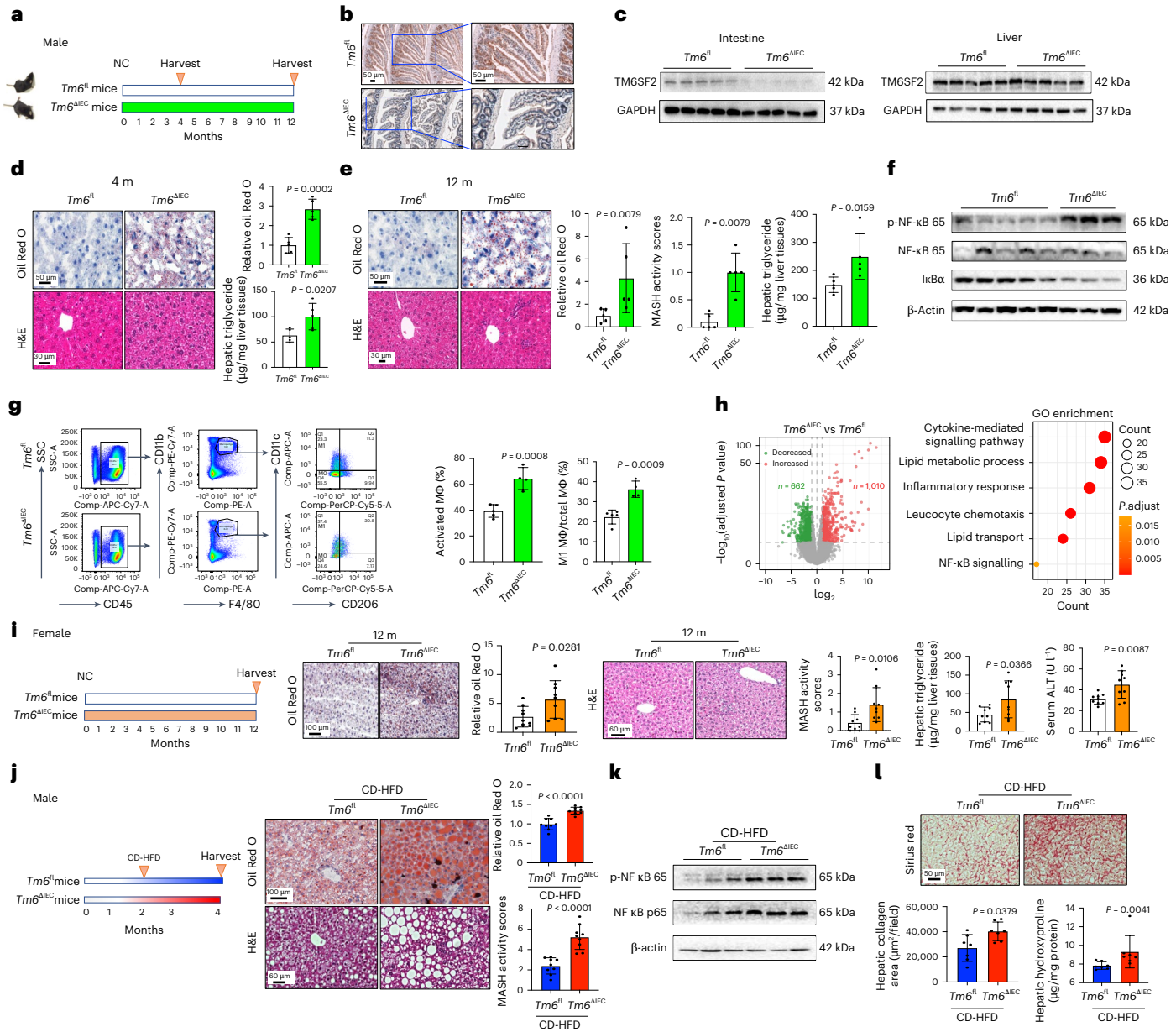

Fig. 1 | Intestinal *Tm6sf2* deficiency in mice triggers MASH. a, Experimental schematic of *Tm6sf2*$^{\Delta IEC}$ and *Tm6sf2*^{fl} male mice fed with NC for 4 or 12 months. **b**,**c**, Representative small intestine images of TM6SF2 immunohistochemistry (**b**), and TM6SF2 protein expression in small intestine and liver tissues (**c**) of *Tm6sf2*$^{\Delta IEC}$ and *Tm6sf2*^{fl} mice ($n = 5$ per group). **d**, Representative liver images of Oil Red O and H&E staining and hepatic triglyceride of *Tm6sf2*$^{\Delta IEC}$ and *Tm6sf2*^{fl} mice fed with NC for 4 months ($n = 5$ per group). **e**–**h**, Representative liver images of Oil Red O and H&E staining with histological scoring and hepatic triglyceride ($n = 5$ per group; **e**) and hepatic protein expression of NF-κB pathway markers (*Tm6sf2*$^{\Delta IEC}$, $n = 3$; *Tm6sf2*^{fl}, $n = 5$; **f**), flow cytometric analysis of hepatic macrophage (MΦ) populations (*Tm6sf2*$^{\Delta IEC}$, $n = 4$; *Tm6sf2*^{fl}, $n = 5$; **g**) and volcano plot and Gene Ontology enrichment analysis of RNA sequencing on liver tissues ($n = 5$ per group; **h**) of *Tm6sf2*$^{\Delta IEC}$ and *Tm6sf2*^{fl} mice at 12 months of age. **i**, Experimental schematic, representative hepatic images of Oil Red O and H&E staining with histological scoring and hepatic triglyceride and serum ALT levels of *Tm6sf2*$^{\Delta IEC}$ and *Tm6sf2*^{fl} female mice fed with NC for 12 months ($n = 9$ per group). **j**,**k**, Experimental schematic and representative liver images of Oil Red O and H&E staining with histological scoring ($n = 9$ per group; **j**) and hepatic protein expression of NF-κB pathway markers ($n = 3$ per group; **k**) of *Tm6sf2*$^{\Delta IEC}$ and *Tm6sf2*^{fl} male mice fed with CD-HFD for 2 months. **l**, Representative liver images of Sirius Red staining and hepatic hydroxyproline of *Tm6sf2*$^{\Delta IEC}$ and *Tm6sf2*^{fl} mice fed with CD-HFD for 14 months ($n = 7$ per group). Results are presented as the mean ± s.d. Statistical significance was determined by two-tailed Student's *t*-test (**d**, **g**, **i** and **j**), two-tailed Mann–Whitney *U* test (**e** and **l**), DESeq2 (**h**, left) or clusterProfiler (**h**, right). *Tm6*, *Tm6sf2*.

lipid processing in the small intestine[9], the role of intestinal TM6SF2 in MASH remains unknown.

Apart from host genetics, we previously reported that the gut microbiota could drive MASH development in mice through impairing the intestinal barrier and elevating production of harmful metabolites[10,11]. Another study found that individuals with MASLD harbouring the *TM6SF2* variant have increased levels of the endotoxaemia marker lipopolysaccharide (LPS)-binding protein (LBP)[12]. Nevertheless, it is unclear whether and how intestinal TM6SF2 affects the gut microbiota and intestinal barrier to contribute to MASH development.

Herein, we investigated the role of intestinal *Tm6sf2* in MASH development by specifically deleting *Tm6sf2* in small intestinal epithelial cells (IECs) of mice (*Tm6sf2*$^{\Delta IEC}$). The effects of intestinal *Tm6sf2* deficiency on intestinal barrier integrity, gut microbiota and

https://doi.org/10.1038/s42255-024-01177-7

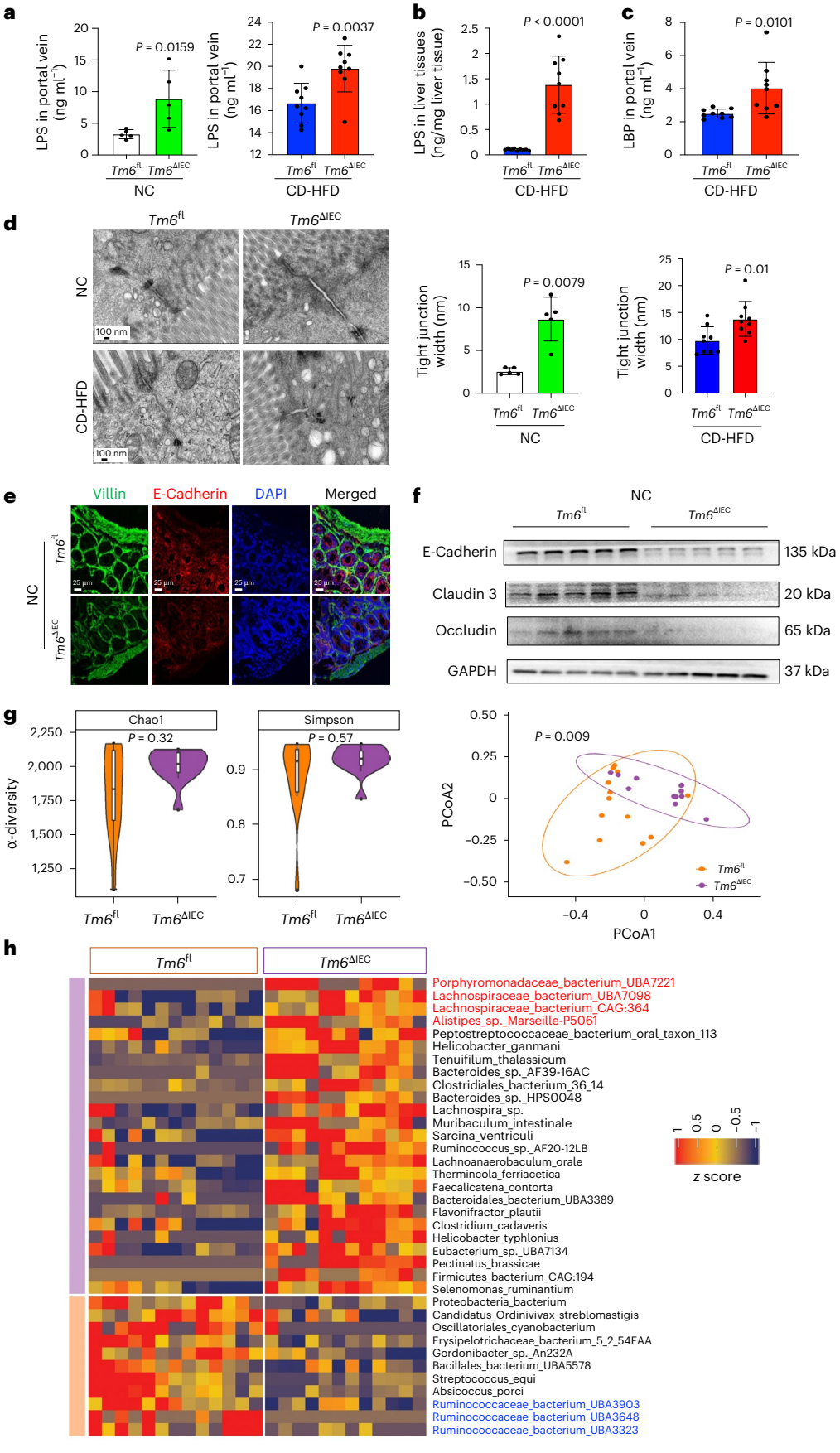

metabolites were examined. Mechanistically, intestinal Tm6sf2 could directly bind to fatty acid-binding protein (FABP) 5 to regulate the secretion of long-chain fatty acids (LCFAs) and influence microbiota composition. The significance of the gut microbiota in MASH induced by intestinal *Tm6sf2* deficiency was testified by transplanting stools from *Tm6sf2*$^{\Delta IEC}$ mice to germ-free mice. In addition, we evaluated the therapeutic potential of targeting gut microbiota or toxic metabolites against MASH.

Fig. 2 | Intestine *Tm6sf2* deficiency results in intestinal barrier dysfunction and gut microbiota dysbiosis. a,**b**, LPS level in portal vein serum (**a**) and liver tissues (**b**) of *Tm6sf2*$^{\Delta IEC}$ and *Tm6sf2*^{fl} mice fed with NC ($n = 5$ per group) or CD-HFD ($n = 9$ per group). **c**, LBP level in portal vein serum of *Tm6sf2*$^{\Delta IEC}$ and *Tm6sf2*^{fl} mice fed with CD-HFD ($n = 9$ per group). **d**, Transmission electron microscopy of *Tm6sf2*$^{\Delta IEC}$ and *Tm6sf2*^{fl} mice fed with NC at age 12 months ($n = 5$ per group) or CD-HFD for 2 months ($n = 9$ per group). **e**,**f**, Representative small intestine images of immunofluorescence staining for E-cadherin (red), villin (green) and DAPI (blue; **e**), and expression of intestinal barrier proteins in the small intestine (**f**) of NC-fed *Tm6sf2*$^{\Delta IEC}$ and *Tm6sf2*^{fl} mice ($n = 5$ per group) **g**, α-diversity (Chao1 or Simpson) and β-diversity between NC-fed *Tm6sf2*$^{\Delta IEC}$ ($n = 12$) and *Tm6sf2*^{fl} ($n = 13$) mice. The central horizontal line denotes the 50th percentile, while the box contains the 25th to 75th percentiles of the dataset. The whiskers mark the 5th and 95th percentiles. Data from two replicates were combined for analysis. **h**, Heat map of differential faecal microorganisms between *Tm6sf2*$^{\Delta IEC}$ ($n = 12$) and *Tm6sf2*^{fl} ($n = 13$) mice. Results are presented as the mean ± s.d. Statistical significance was determined by two-tailed Student's *t*-test (**a**, right; **b**; **c** and **d**, right), two-tailed Mann–Whitney *U* test (**a**, left and **d**, left), Wilcoxon test (**g**, left) or Adonis test (**g**, right).

Results

Systemic *Tm6sf2* deletion triggers MASH in mice

To investigate the role of Tm6sf2 in MASH, we generated systemic *Tm6sf2* knockout (KO) mice that were fed a normal chow (NC) or a choline-deficient high-fat diet (CD-HFD; Extended Data Fig. 1a–c,g). Compared to wild-type mice, systemic *Tm6sf2* KO mice fed with NC displayed more severe steatosis, oxidative stress and liver injury, as evidenced by elevated MASH activity score (Extended Data Fig. 1d), triglyceride content, lipid peroxidation (Extended Data Fig. 1e) and serum alanine aminotransferase (ALT) level (Extended Data Fig. 1f). Similarly, CD-HFD-fed systemic *Tm6sf2* KO mice displayed more pronounced steatohepatitis than CD-HFD wild-type mice, as evidenced by increased MASH activity score (Extended Data Fig. 1g), lipid peroxidation (Extended Data Fig. 1h) and serum ALT level (Extended Data Fig. 1i).

To examine the role of hepatic Tm6sf2 in MASH, we generated liver-specific *Tm6sf2* KO (*Tm6sf2*$^{\Delta Liver}$) mice to specifically delete *Tm6sf2* in mouse liver (Extended Data Fig. 2a). The loss of *Tm6sf2* in the liver of *Tm6sf2*$^{\Delta Liver}$ mice was confirmed by immunohistochemistry (Extended Data Fig. 2b) and western blot (Extended Data Fig. 2c). Compared to *Tm6sf2*^{fl} wild-type littermates, *Tm6sf2*$^{\Delta Liver}$ mice exhibited significantly increased hepatic lipid accumulation (Extended Data Fig. 2d,e). However, neither feeding of NC nor CD-HFD to *Tm6sf2*$^{\Delta Liver}$ mice led to a significant increase in MASH activity score or lipid peroxidation (Extended Data Fig. 2d–g), whereas CD-HFD-fed *Tm6sf2*$^{\Delta Liver}$ mice had higher serum ALT levels than CD-HFD-fed wild-type controls (Extended Data Fig. 2h). These findings thus suggest that systemic *Tm6sf2* deficiency has stronger pro-steatohepatitic effects than liver-specific *Tm6sf2* deficiency, implying the involvement of non-hepatic Tm6sf2 in MASH development.

Intestinal *Tm6sf2* deficiency triggers MASH in mice

TM6SF2 is mainly expressed in human liver and small intestine, while the latter has higher expression[9]. To evaluate whether intestinal Tm6sf2 plays a role in MASH, we generated IEC-specific *Tm6sf2* KO (*Tm6sf2*$^{\Delta IEC}$) mice fed with NC for 4 months or 12 months (Fig. 1a). The loss of intestinal but not liver *Tm6sf2* in *Tm6sf2*$^{\Delta IEC}$ mice was confirmed by immunohistochemistry staining and western blot (Fig. 1b,c). *Tm6sf2*$^{\Delta IEC}$ mice at 4 months old spontaneously developed MASLD, as evidenced by elevated hepatic lipid accumulation ($P = 0.0002$) and triglyceride content ($P = 0.0207$) compared to *Tm6sf2*^{fl} wild-type mice (Fig. 1d). More severe MASH was also observed in *Tm6sf2*$^{\Delta IEC}$ mice at 12 months old with increased MASH activity score ($P = 0.0079$), as well as elevated hepatic lipid accumulation ($P = 0.0079$) and triglyceride content ($P = 0.0159$) compared to *Tm6sf2*^{fl} wild-type controls (Fig. 1e).

Hepatic levels of pro-inflammatory cytokine tumour necrosis factor (TNF) were upregulated in *Tm6sf2*$^{\Delta IEC}$ mice compared to *Tm6sf2*^{fl} wild-type controls, together with enhanced nuclear factor κB (NF-κB) activation by increased phosphor-p65 NF-κB subunit and decreased IκBα (Extended Data Fig. 3a and Fig. 1f). Because TNF is mainly secreted by macrophages[13], flow cytometry was conducted to analyse macrophage subtypes in mouse liver tissues (Supplementary Fig. 1). The proportions of activated macrophages and M1 pro-inflammatory macrophages ($CD45^+F4/80^+CD11b^+CD11c^+CD206^-$) were significantly increased in *Tm6sf2*$^{\Delta IEC}$ mice compared to *Tm6sf2*^{fl} wild-type controls (both $P < 0.001$; Fig. 1g). These results were confirmed by RNA sequencing on liver tissues of *Tm6sf2*$^{\Delta IEC}$ and *Tm6sf2*^{fl} littermates, showing activation of multiple MASH-related pathways including cytokine-mediated signalling, lipid metabolic process and NF-κB signalling (Fig. 1h and Extended Data Fig. 3b).

To determine whether these observations were sex dependent, we assessed the effects of intestinal Tm6sf2 on MASH in female mice. In line with the results from male mice, female *Tm6sf2*$^{\Delta IEC}$ mice displayed significantly elevated hepatic lipid accumulation ($P = 0.0281$) and increased MASH activity scores ($P = 0.0106$), as well as elevated triglyceride content ($P = 0.0366$) and serum ALT level ($P = 0.0087$), compared to female *Tm6sf2*^{fl} wild-type controls (Fig. 1i). Collectively, these findings demonstrate that intestine-specific *Tm6sf2* deficiency spontaneously triggers MASH with increased hepatic inflammation in both male and female mice.

Intestinal *Tm6sf2* deficiency accelerates diet-induced MASH

We also investigated whether intestinal *Tm6sf2* deficiency could aggravate diet-induced MASH by supplementing *Tm6sf2*$^{\Delta IEC}$ and *Tm6sf2*^{fl} mice with a CD-HFD for 2 months. Indeed, more pronounced steatohepatitis was developed in CD-HFD-fed *Tm6sf2*$^{\Delta IEC}$ mice compared to CD-HFD-fed *Tm6sf2*^{fl} wild-type controls, as shown by elevated hepatic lipid accumulation ($P < 0.0001$) and MASH activity score ($P < 0.0001$; Fig. 1j). Upregulated NF-κB activation (increased p-NF-κB p65 protein) and pro-inflammatory cytokine secretion (TNF and interleukin (IL)-6) were also observed in the livers of CD-HFD-fed *Tm6sf2*$^{\Delta IEC}$ mice (Fig. 1k and Extended Data Fig. 3c). Moreover, CD-HFD-fed *Tm6sf2*$^{\Delta IEC}$ mice had significantly higher collagen deposition ($P = 0.0379$) and hepatic hydroxyproline levels ($P = 0.0041$) than CD-HFD-fed wild-type controls (Fig. 1l).

Fig. 3 | Intestinal *Tm6sf2* deficiency promotes MASH by inducing metabolite alteration. a,**b**, PCA and PLS-DA of untargeted metabolomic profiling (**a**), and heat map of differential metabolites (**b**) in stools ($n = 5$ per group), portal vein serum ($n = 4$ per group) and liver tissues ($n = 5$ per group) of NC-fed *Tm6sf2*$^{\Delta IEC}$ and *Tm6sf2*^{fl} mice. **c**, LPA-targeted metabolomics on portal vein serum of *Tm6sf2*$^{\Delta IEC}$ and *Tm6sf2*^{fl} mice fed with NC ($n = 4$ per group), CD-HFD ($n = 9$ per group) or HFHC diet ($n = 7$ per group). **d**, LPA-targeted metabolomics on liver tissues of mice fed with NC ($n = 4$ per group) or HFHC diet ($n = 7$ per group). **e**, Correlation analysis between differential bacteria and LPA levels in stools, portal vein serum and liver tissues of *Tm6sf2*$^{\Delta IEC}$ and *Tm6sf2*^{fl} mice. $^*P < 0.05$, $^{**}P < 0.01$. **f**, LPS-targeted metabolomics in stools, portal vein serum and liver tissues of germ-free mice gavaged with Lachnospiraceae for 10 days ($n = 5$ per group). **g**,**h**, Representative images of Oil Red O staining with stained area normalized to cell number ($n = 5$ per group), cellular triglyceride and lipid peroxidation normalized to total protein content ($n = 3$ per group), and supernatant TNF level ($n = 3$ per group) of AML-12 mouse normal hepatocytes (**g**) or THLE-2 human normal hepatocytes (**h**) under LPA treatment with or without LPAR inhibitor AM095. Results are presented as the mean ± s.d. Statistical significance was determined by Adonis test (**a**), two-tailed Student's *t*-test (**c**, **d** and **f**, left and right), two-tailed Mann–Whitney *U* test (**f**, middle), Spearman's correlation analysis (**e**) or one-way analysis of variance (ANOVA) followed by Turkey's multiple comparison (**g** and **h**).

https://doi.org/10.1038/s42255-024-01177-7

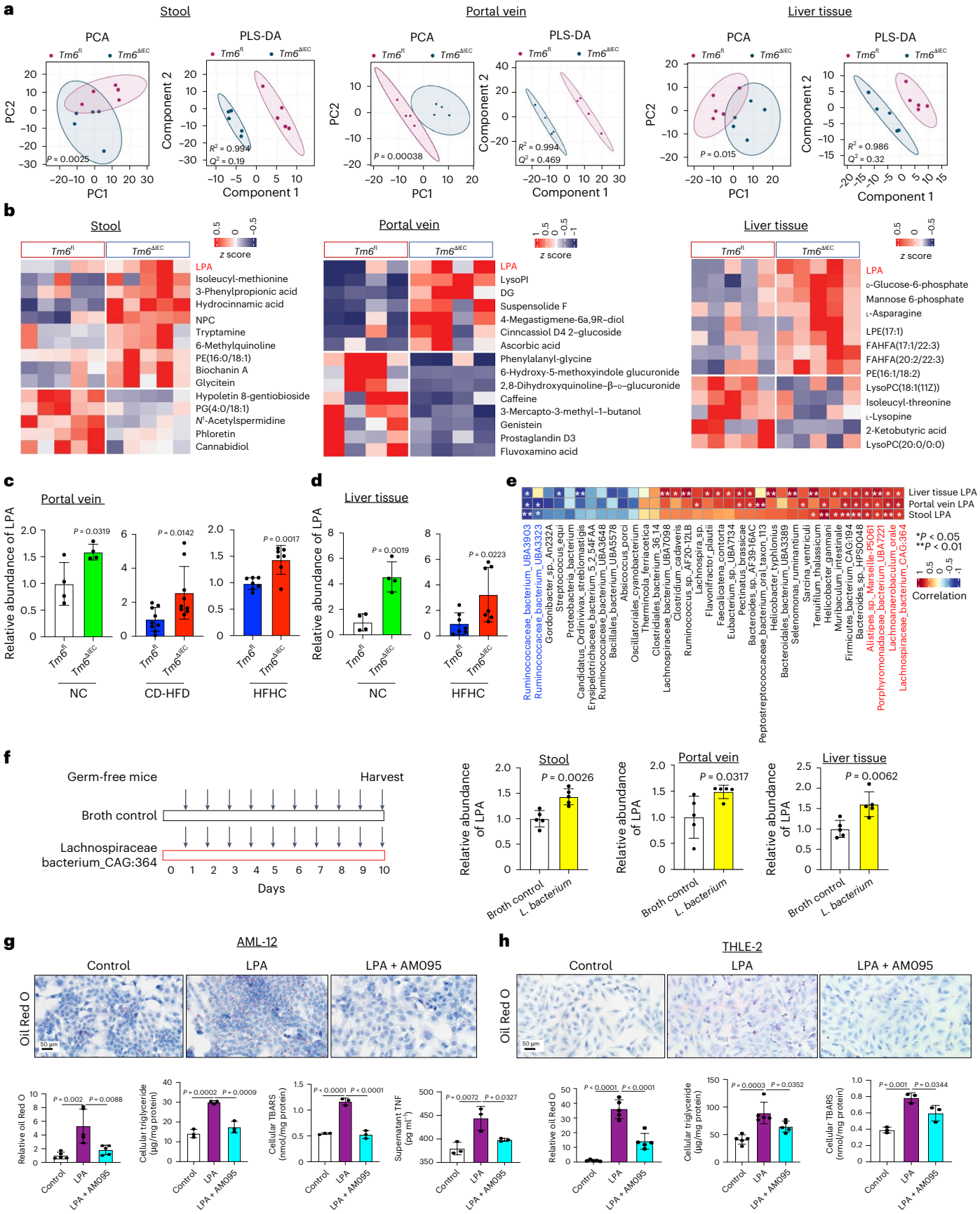

https://doi.org/10.1038/s42255-024-01177-7

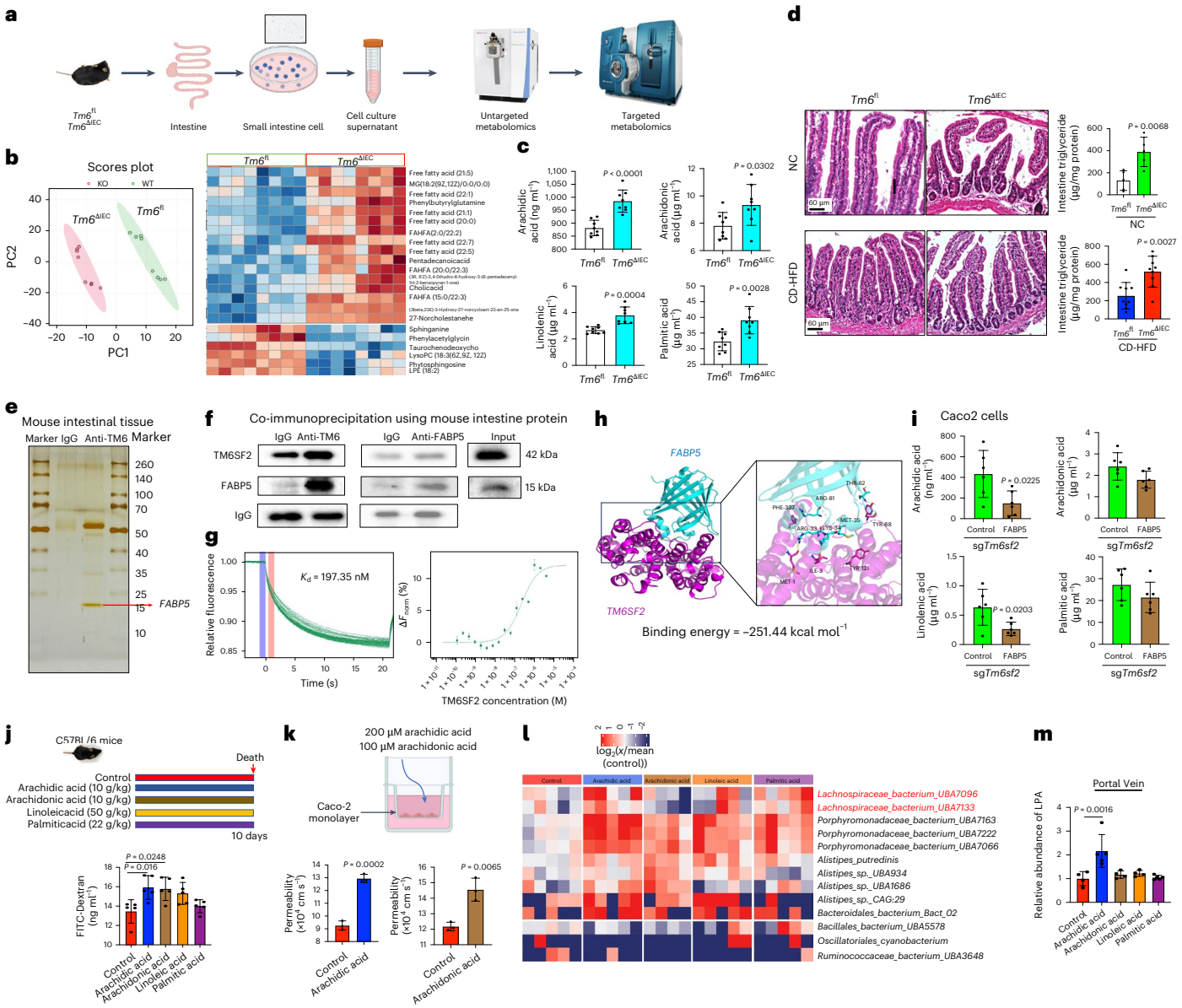

Fig. 4 | Intestinal cells with *Tm6sf2* deficiency secrete free fatty acids to induce gut microbiota dysbiosis. a, Experimental schematic of untargeted metabolomic profiling on the culture supernatant of IECs isolated from *Tm6sf2*$^{\Delta IEC}$ and *Tm6sf2*^{fl} mice. Created with BioRender.com. **b**, PCA analysis and heat map of differential metabolites secreted by IECs from mice ($n = 8$ per group). **c**, Metabolomics targeting free fatty acids on the cultural supernatant of isolated IECs ($n = 8$ per group). **d**, Representative small intestine images of H&E staining and intestinal triglyceride of *Tm6sf2*$^{\Delta IEC}$ mice fed with NC ($n = 5$ per group) or CD-HFD ($n = 9$ per group). **e**, Silver staining coupled with mass spectrometry analysis after pull-down assay on mouse intestinal tissues. **f**, Co-immunoprecipitation of TM6SF2 and FABP5 using mouse intestinal proteins. **g**, MST assay for direct binding between TM6SF2 and FABP5 with dissociation constant (K_d) provided. **h**, Representative structure of molecular docking between TM6SF2 (purple) and FABP5 (blue). **i**, Metabolomics targeting free fatty acids in *TM6SF2* KO Caco2 cells with or without FABP5 overexpression ($n = 6$ per group). **j**, Experimental schematic and intestinal permeability by FITC-labelled dextran assay in mice supplemented with the top differential free fatty acids ($n = 5$ per group). **k**, Permeability of Caco2 cell monolayers treated with arachidic acid or arachidonic acid ($n = 3$ per group). **l**,**m**, Heat map of differential faecal microorganisms (**l**) and LPA-targeting metabolomics on portal vein serum (**m**) of mice treated with free fatty acids ($n = 4$–5 per group). Results are presented as the mean ± s.d. Experiments were repeated three times with similar results (**e** and **f**). Statistical significance was determined by two-tailed Student's *t*-test (**c**, **d**, **i** and **k**) or one-way ANOVA followed by Turkey's multiple comparison (**j** and **m**).

For confirmation, we established another mouse model of diet-induced MASH by feeding *Tm6sf2*$^{\Delta IEC}$ and *Tm6sf2*^{fl} mice with a high-fat high-cholesterol (HFHC) diet for 2 months (Extended Data Fig. 4a). As expected, HFHC-fed *Tm6sf2*$^{\Delta IEC}$ mice developed more severe steatohepatitis than HFHC-fed *Tm6sf2*^{fl} wild-type controls, as shown by elevated MASH activity score (Extended Data Fig. 4b). Together, our consistent findings from multiple mouse models indicate that intestinal *Tm6sf2* deficiency plays a critical role in promoting the development of spontaneous or diet-induced MASH in mice.

Intestinal *Tm6sf2* deficiency impairs the intestinal barrier

Human intestine and liver communicate through the gut–liver axis, while an impaired intestinal barrier is the prerequisite for MASH development[14]; therefore, we speculated that intestinal *Tm6sf2* deficiency may influence the intestinal barrier. Indeed, portal vein (Fig. 2a) and liver LPS levels (Fig. 2b) were significantly elevated in *Tm6sf2*$^{\Delta IEC}$ mice fed with NC or CD-HFD, compared with corresponding *Tm6sf2*^{fl} wild-type controls. Serum level of LBP, the binding protein of LPS, was also upregulated in the portal vein of *Tm6sf2*$^{\Delta IEC}$ mice fed with a CD-HFD (Fig. 2c).

https://doi.org/10.1038/s42255-024-01177-7

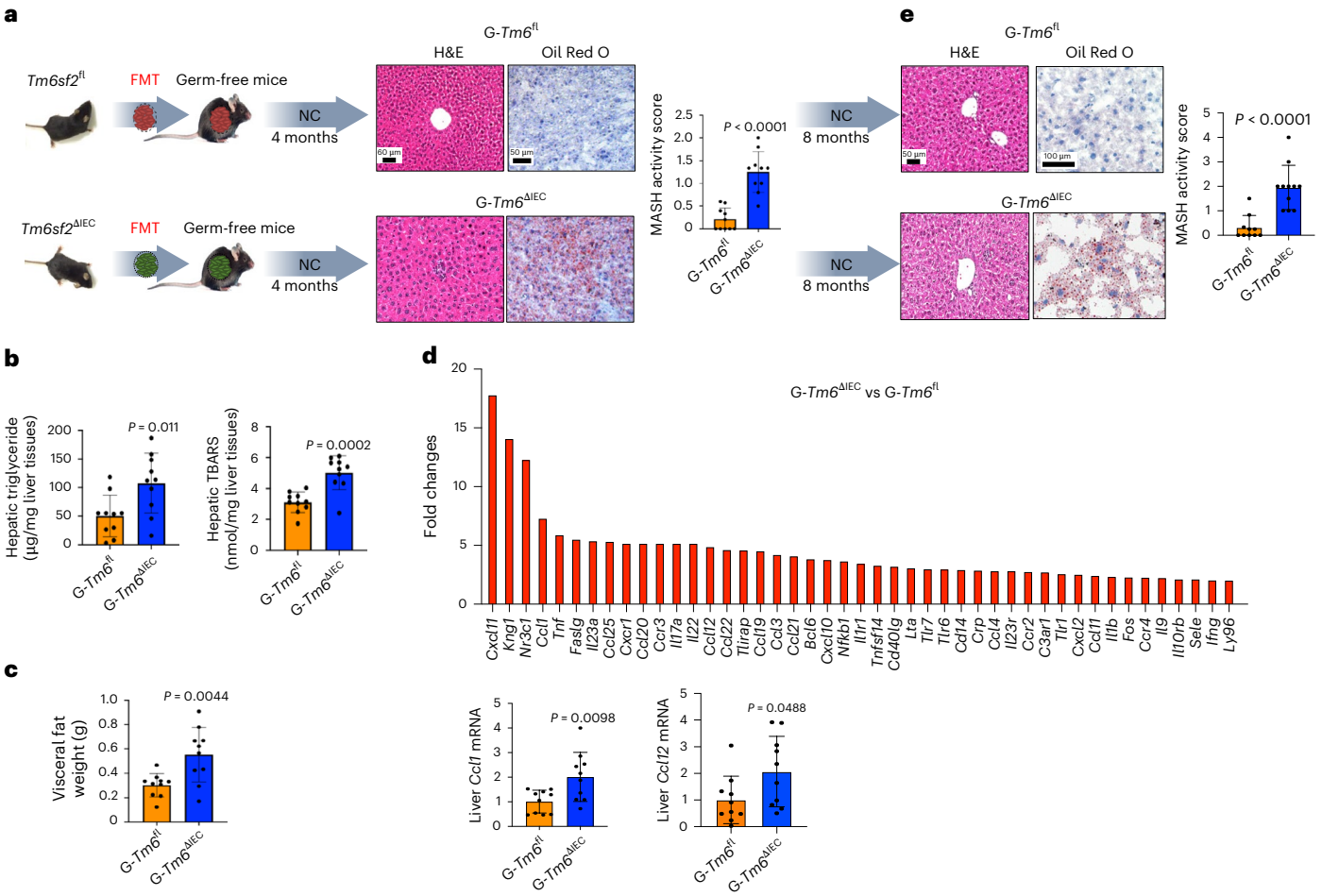

Fig. 5 | Gut microbiota from *Tm6sf2*$^{\Delta IEC}$ mice promotes NASH development in germ-free mice. a, Schematic of FMT experiment and representative images of Oil Red O and H&E staining with histological scoring in male germ-free mice transplanted with stools from *Tm6sf2*$^{\Delta IEC}$ (G-*Tm6sf2*$^{\Delta IEC}$) or *Tm6sf2*^{fl} (G-*Tm6sf2*^{fl}) and fed with NC for 4 or 8 months ($n = 10–11$ per group). **b**–**d**, Hepatic triglyceride and lipid peroxidation (**b**), visceral fat (**c**) and PCR array and *Ccl1* and *Ccl12* mRNA levels in liver tissues (**d**) of G-*Tm6sf2*$^{\Delta IEC}$ and G-*Tm6sf2*^{fl} mice 4 months after FMT ($n = 10$ per group). **e**, Representative images of Oil Red O and H&E staining with histological scoring in G-*Tm6sf2*$^{\Delta IEC}$ ($n = 11$) and G-*Tm6sf2*^{fl} ($n = 10$) 8 months after FMT. Results are presented as the mean ± s.d. Statistical significance was determined by two-tailed Student's *t*-test (**b** and **c**) and two-tailed Mann–Whitney *U* test (**a** and **e**). TBARS, thiobarbituric acid-reactive substances assay.

In keeping with this, transmission electron microscopy revealed abnormalities of intestinal intracellular junctions in *Tm6sf2*$^{\Delta IEC}$ mice with a widened apical junctional complex and paracellular gap (Fig. 2d and Extended Data Fig. 4c). Moreover, intestinal expressions of adherent protein E-cadherin and tight junction proteins claudin 3 and occludin were all markedly downregulated in *Tm6sf2*$^{\Delta IEC}$ mice (Fig. 2e,f). For further confirmation, we deleted *TM6SF2* expression in human colon epithelial cell line Caco2. The results showed that *TM6SF2* deletion led to increased permeability of in vitro monolayers of colon epithelial cells (Extended Data Fig. 5). Collectively, these findings indicate that intestinal *Tm6sf2* deficiency induces intestinal barrier dysfunction.

Intestinal *Tm6sf2* deficiency induces gut microbial dysbiosis

Given that the gut microbiota plays an important role in shaping the structure and integrity of intestinal barrier[15], we performed shotgun metagenomic sequencing on faecal samples of *Tm6sf2*$^{\Delta IEC}$ and *Tm6sf2*^{fl} mice. Principal component analysis (PCA) revealed that the microbial community was significantly different between *Tm6sf2*$^{\Delta IEC}$ and *Tm6sf2*^{fl} wild-type mice ($P = 0.009$; Fig. 2g). Differential bacterial taxa were also identified (Fig. 2h). Potentially pathogenic bacteria including *Porphyromonadaceae bacterium* UBA 7221, Lachnospiraceae *bacterium* UBA7098, *L. bacterium* CAG:364 and *Alistipes* sp. *Marseille* P5061 were markedly enriched in *Tm6sf2*$^{\Delta IEC}$ mice, accompanied by the depletion of protective bacteria *Ruminococcaceae bacterium* UBA3323, UBA3648 and UBA3903 (Fig. 2h).

Elevated LPA promotes MASH in mice with intestinal *Tm6sf2* deficiency

The liver is exposed to metabolites in the portal vein that are derived from gut microorganisms[16]. To evaluate metabolite changes, we performed untargeted metabolomic profiling on stools, portal vein serum and liver tissues of *Tm6sf2*$^{\Delta IEC}$ and *Tm6sf2*^{fl} mice. PCA and partial least-squares discriminant analysis (PLS-DA) revealed that the metabolome profile was significantly different between *Tm6sf2*$^{\Delta IEC}$ and *Tm6sf2*^{fl} wild-type mice in all three types of samples (Fig. 3a). Among all differential metabolites, LPA was the top metabolite consistently upregulated in stools, portal vein serum and liver tissues of *Tm6sf2*$^{\Delta IEC}$ mice (Fig. 3b). This was validated by targeted metabolomics, which confirmed the significant elevation of LPA in the portal vein serum of NC-fed, CD-HFD-fed or HFHC-fed *Tm6sf2*$^{\Delta IEC}$ mice (Fig. 3c). LPA level was also increased in liver tissues of NC-fed or HFHC-fed *Tm6sf2*$^{\Delta IEC}$ mice, compared to *Tm6sf2*^{fl} littermates (Fig. 3d).

The correlation between differential microorganisms and metabolites under intestinal *Tm6sf2* deficiency was determined. Integrative analysis revealed that LPA levels in stools, portal vein serum and liver tissues were positively correlated with enriched bacteria including

https://doi.org/10.1038/s42255-024-01177-7

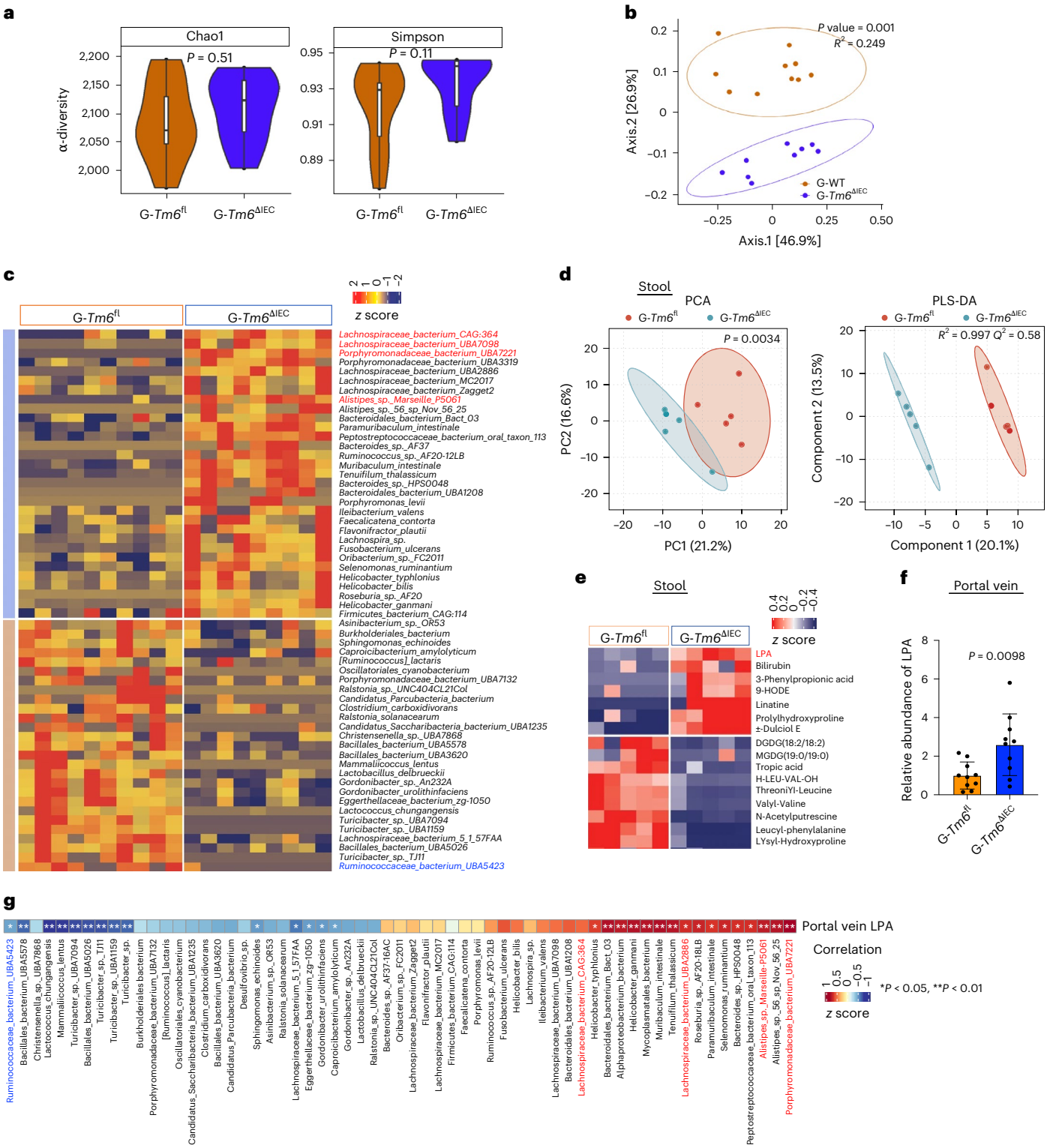

Fig. 6 | Gut microbiota and metabolomics in germ-free mice transplanted with stools from *Tm6sf2*$^{\Delta IEC}$ mice. a, α-diversity (Chao1 or Simpson) between G-*Tm6sf2*$^{\Delta IEC}$ ($n = 9$) and G-*Tm6sf2*^{fl} ($n = 10$) mice. The central horizontal line denotes the 50th percentile, while the box contains the 25th to 75th percentiles of the dataset. The whiskers mark the 5th and 95th percentiles. **b**,**c**, β-diversity (**b**) and heat map of differential faecal microorganisms (**c**) between G-*Tm6sf2*$^{\Delta IEC}$ ($n = 9$) and G-*Tm6sf2*^{fl} ($n = 10$) mice. **d**,**e**, PCA and PLS-DA analyses (**d**), and heat map of differential metabolites (**e**) identified by untargeted metabolomic profiling on stools of G-*Tm6sf2*$^{\Delta IEC}$ and G-*Tm6sf2*^{fl} mice ($n = 5$ per group). **f**, LPA-targeting metabolomics on portal vein serum of G-*Tm6sf2*$^{\Delta IEC}$ and G-*Tm6sf2*^{fl} mice ($n = 10$ per group). **g**, Correlation analysis between differential bacteria and portal vein LPA in G-*Tm6sf2*$^{\Delta IEC}$ ($n = 9$) and G-*Tm6sf2*^{fl} ($n = 10$) mice. $^{*}P < 0.05$, $^{**}P < 0.01$. Results are presented as the mean ± s.d. Statistical significance was determined by Wilcoxon test (**a**), Adonis test (**b** and **d**), two-tailed Student's *t*-test (**f**) or Spearman's rank correlation coefficient (**g**). *P* value was adjusted in **g**.

https://doi.org/10.1038/s42255-024-01177-7

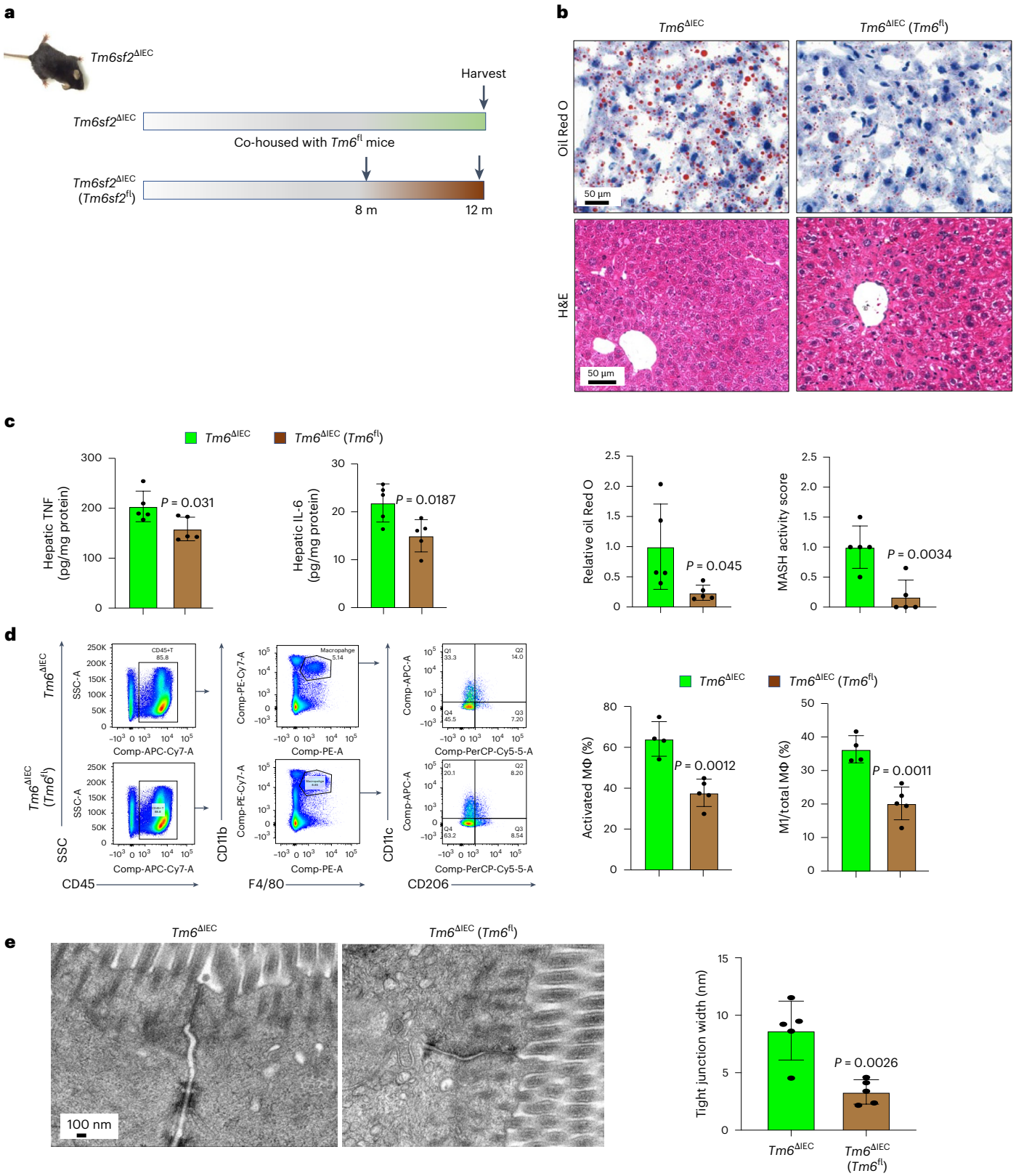

Fig. 7 | Gut microbiota modulation improves MASH induced by intestinal *Tm6sf2* deficiency. a, Experimental schematic of microbiota modulation by co-housing male *Tm6sf2*$^{\Delta IEC}$ mice with male *Tm6sf2*^{fl} mice for 4 months to restore the gut microbiota ($n = 5$ per group). **b**–**e**, Representative images of Oil Red O and H&E staining with histological scoring (**b**), hepatic levels of TNF and IL-6 (**c**), flow cytometric analysis of hepatic immune cell populations (**d**) and transmission electron microscopy (**e**) in *Tm6sf2*$^{\Delta IEC}$ and co-housed *Tm6sf2*$^{\Delta IEC}$ mice ($n = 5$ per group). Results are presented as the mean ± s.d. Statistical significance was determined by two-tailed Student's *t*-test (**b**–**e**).

Lachnospiraceae, Porphyromonadaceae and *Alistipes*, while negatively correlated with Ruminococcaceae (Fig. 3e). Prediction analysis on microbial functional pathways showed that Lachnospiraceae, Porphyromonadaceae and *Alistipes* encoded the enzyme gene *gpsA* which is involved in the conversion of glycerone phosphate to sn-glycerol 3-phosphate, a precursor of LPA and catalyst of de novo synthesis of glycerolipids[17]. Lachnospiraceae and *Alistipes* also encoded the enzyme gene *plsY*, which could further catalyse the conversion of sn-glycerol 3-phosphate to LPA (Extended Data Fig. 6a,b). Hence, these results imply the potential of these enriched bacteria to produce LPA under intestinal *Tm6sf2* deficiency. Considering the significant enrichment of Lachnospiraceae in stools of individuals with MASLD[18], its strong correlation with LPA biosynthesis (Fig. 3e) and its presence of LPA-producing enzymes (Extended Data Fig. 6a,b), we supplemented *L. bacterium* to germ-free wild-type mice via oral gavage. Compared to mice treated with broth control, *L. bacterium*-treated mice had significantly higher levels of LPA in their stools, portal vein serum and liver tissues (Fig. 3f), thus suggesting that LPA elevation is at least partially derived from enriched bacteria such as Lachnospiraceae in *Tm6sf2*$^{\Delta IEC}$ mice.

The in vitro role of LPA was investigated. LPA treatment significantly induced triglyceride accumulation, lipid peroxidation and inflammation in mouse normal hepatocytes AML-12 (Fig. 3g). Similarly, increased lipid accumulation and lipid peroxidation were observed in human normal hepatocytes THLE-2 after LPA treatment (Fig. 3h). LPA receptor (LPAR) is the receptor of LPA in hepatocytes[19]. Therefore, we applied LPAR antagonist AM095 to cells, in addition to LPA treatment. LPAR blockade markedly reversed LPA-induced lipid accumulation, lipid peroxidation and inflammation in mouse AML-12 and human THLE-2 cells (Fig. 3g,h). Together, our findings illustrate that intestinal *Tm6sf2* deficiency alters the gut microbiota and increases LPA production, while the latter could enter the liver through the portal vein circulation to promote MASH development.

Tm6sf2-deficient IECs secrete LCFAs to induce gut dysbiosis

To decipher the underlying mechanism of intestinal *Tm6sf2* deficiency in MASH, we isolated primary IECs from the small intestines of *Tm6sf2*$^{\Delta IEC}$ and *Tm6sf2*^{fl} mice and performed untargeted metabolomics on the culture supernatant (Fig. 4a). Our analysis identified that metabolites secreted by IECs from *Tm6sf2*$^{\Delta IEC}$ and *Tm6sf2*^{fl} mice were significantly different, with free fatty acids being the top differential metabolites (Fig. 4b). This was confirmed by targeted metabolomics, of which LCFAs including arachidic acid ($P < 0.0001$), arachidonic acid ($P = 0.0302$), linoleic acid ($P = 0.0004$) and palmitic acid ($P = 0.0028$) were significantly upregulated in the culture supernatant of IECs isolated from *Tm6sf2*$^{\Delta IEC}$ mice (Fig. 4c). In addition, significantly increased lipid accumulation was observed in the small intestines of *Tm6sf2*$^{\Delta IEC}$ mice fed with NC, CD-HFD and HFHC (Fig. 4d and Extended Data Fig. 4d).

We next explored how intestinal *Tm6sf2* deficiency triggers the release of free fatty acids in the intestinal epithelium. Through silver staining coupled with mass spectrometry, we identified that FABP5 was a potential interacting partner of Tm6sf2 in mouse intestinal tissues (Fig. 4e and Supplementary Table 1). Co-immunoprecipitation experiments showed that anti-TM6SF2 could pull down FABP5, and anti-FABP5 could reciprocally pull down TM6SF2, thus confirming their interaction (Fig. 4f). The direct interplay between TM6SF2 and FABP5 was also validated by microscale thermophoresis (MST) assay, with a dissociation constant of 197.35 nM (Fig. 4g). Molecular docking analysis revealed that TM6SF2 bound to FABP5 through hydrogen bonding and alkyl interactions, with a binding energy of −251.44 kcal mol^{-1} (Fig. 4h). Overexpression of FABP5 in human colon epithelial cells (Caco2) abrogated TM6SF2 KO-induced secretion of LCFAs (Fig. 4i), further demonstrating that TM6SF2 regulates LCFA secretion via FABP5. Meanwhile, intestinal expression of proteins related to lipid transport (NPC1L1 and CD36) was similar between *Tm6sf2*$^{\Delta IEC}$ and *Tm6sf2*^{fl} mice (Extended Data Fig. 7). These results indicate that intestinal *Tm6sf2* deficiency interrupts the binding between Tm6sf2 and FABP5, which in turn promotes the secretion of free fatty acids and lipid accumulation in the intestinal epithelium.

The effects of the top enriched free fatty acids under intestinal *Tm6sf2* deficiency (arachidic acid, arachidonic acid, linoleic acid and palmitic acid) on intestinal barrier and gut microbiota were evaluated in mice (Fig. 4j). Supplementation of arachidic acid or arachidonic acid significantly increased intestinal permeability in mice with elevated efflux of fluorescein isothiocyanate (FITC)-labelled dextran, while no difference was observed in mice treated with linoleic acid or palmitic acid (Fig. 4j). Consistently, arachidic acid and arachidonic acid increased permeability of in vitro monolayers of human colon epithelial cells (Caco2), indicating their capability to impair intestinal barrier integrity (Fig. 4k). These two free fatty acids also induced gut microbial dysbiosis in mice with marked enrichment of LPA-producing Lachnospiraceae (Fig. 4l). Of note, LPA level in portal vein serum was significantly higher only in mice treated with arachidic acid, compared to vehicle controls (Fig. 4m). These findings thus imply that *Tm6sf2*-deficient IECs lead to elevated secretion of free fatty acids, particularly arachidic acid, impaired intestinal barrier and gut dysbiosis with enriched Lachnospiraceae, together promoting LPA biosynthesis and accelerating MASH development.

Gut microbiota of *Tm6sf2*$^{\Delta IEC}$ mice promotes MASH in germ-free mice

To determine whether the gut microbiota plays a crucial role in MASH induced by intestinal *Tm6sf2* deficiency, we transplanted faecal samples from *Tm6sf2*$^{\Delta IEC}$ mice (G-*Tm6sf2*$^{\Delta IEC}$) or *Tm6sf2*^{fl} mice (G-*Tm6sf2*^{fl}) into germ-free mice fed with NC. These germ-free mice were gavaged with stools once at 2 months old and 3 months old, respectively, and were euthanized 4 months or 8 months after the first faecal microbiota transplantation (FMT). G-*Tm6sf2*$^{\Delta IEC}$ mice at 4 months following FMT had significantly higher hepatic lipid accumulation and MASH activity score than G-*Tm6sf2*^{fl} control mice (Fig. 5a). Hepatic triglyceride content ($P = 0.011$) and lipid peroxidation ($P = 0.0002$) were also markedly elevated in G-*Tm6sf2*$^{\Delta IEC}$ mice (Fig. 5b), accompanied by increased visceral fat weight ($P = 0.0044$; Fig. 5c). Enhanced inflammation was confirmed by the upregulated expression of pro-inflammatory cytokines including chemokine ligand (CCL)-1 and CCL12 in G-*Tm6sf2*$^{\Delta IEC}$ mice (Fig. 5d). Consistent results were observed in G-*Tm6sf2*$^{\Delta IEC}$ mice at 8 months following FMT with significantly elevated hepatic lipid accumulation and MASH activity score ($P < 0.0001$; Fig. 5e).

The gut microbiota of recipient germ-free mice was evaluated. Similarly to donor mice, there was no difference in microbial α-diversity, whereas the microbial community was significantly different between

Fig. 8 | Pharmacological inhibition of LPA receptor suppresses MASH. **a**, Experimental schematic of 12-month-old male *Tm6sf2*$^{\Delta IEC}$ mice treated with LPAR inhibitor AM095 (10 mg per kg body weight) or vehicle control twice per week for 6 weeks. **b**,**c**, Representative images of Oil Red O and H&E staining with histological scoring (**b**), and hepatic triglyceride and hepatic lipid peroxidation (**c**) in *Tm6sf2*$^{\Delta IEC}$ mice treated with AM095 or vehicle control ($n = 5$ per group). **d**–**f**, Experimental schematic (**d**), representative images of Oil Red O and H&E staining with histological scoring (**e**), and hepatic triglyceride and serum ALT level (**f**) of male conventional C57BL/6 wild-type mice fed with NC ($n = 5$), MCD diet with vehicle control ($n = 7$), or MCD diet with LPAR inhibitor AM095 ($n = 8$) for 10 days. **g**–**i**, Experimental schematic (**g**), representative images of Oil Red O and H&E staining with histological scoring (**h**) and hepatic triglyceride and lipid peroxidation (**i**) of male C57BL/6 wild-type mice fed with NC ($n = 5$), MCD diet with vehicle control ($n = 5$), or MCD diet with LPAR inhibitor Brp-LPA ($n = 6$). **j**, Overview schematic of the study. Created with BioRender.com. Results are presented as the mean ± s.d. Statistical significance was determined by two-tailed Student's *t*-test (**b** and **c**) or one-way ANOVA followed by Turkey's multiple comparison (**e**, **f**, **h** and **i**). DMSO, dimethylsulfoxide; i.p., intraperitoneal; TBARS, thiobarbituric acid-reactive substances assay.

https://doi.org/10.1038/s42255-024-01177-7

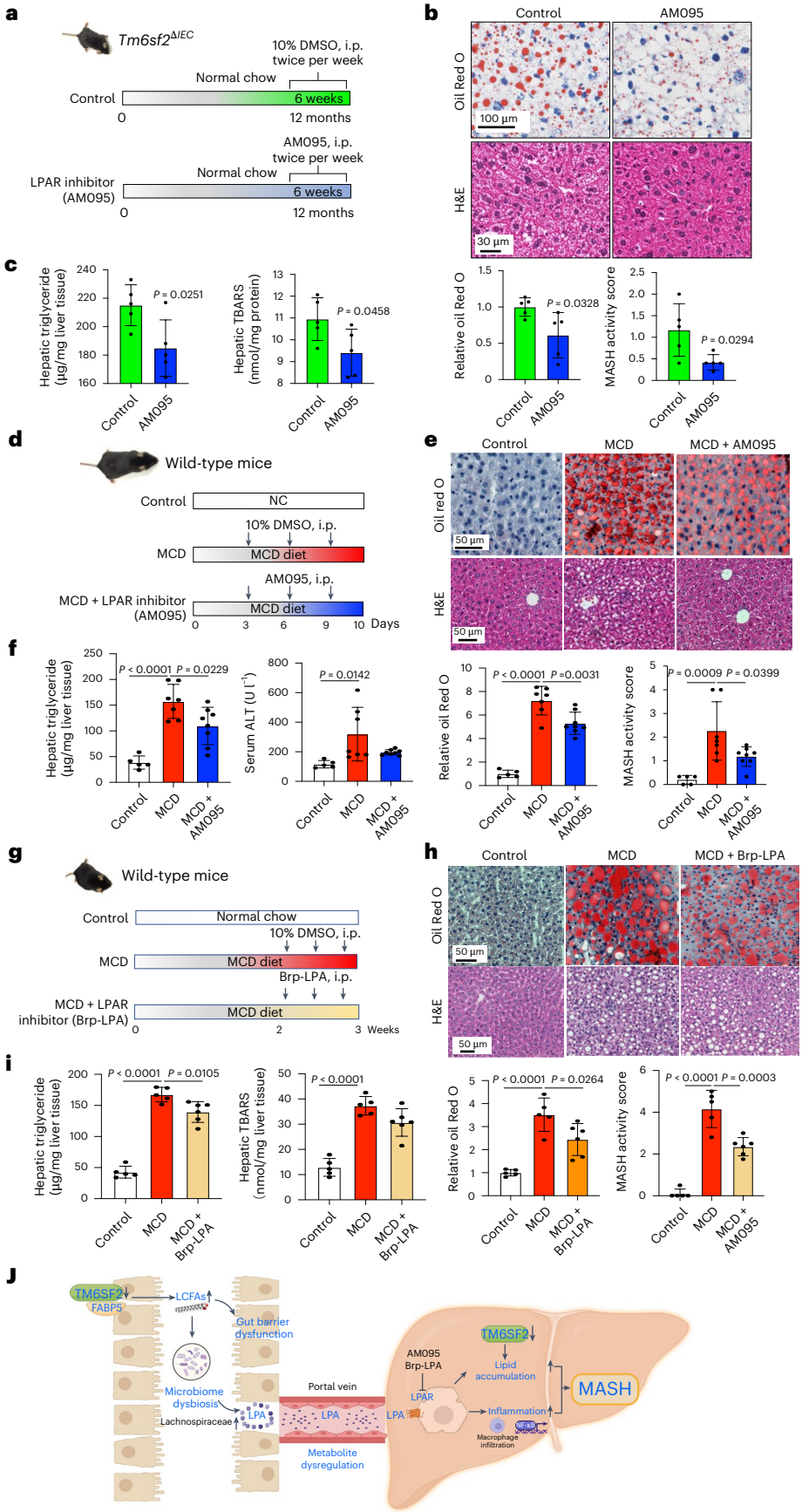

G-*Tm6sf2*$^{\Delta IEC}$ and G-*Tm6sf2*^{fl} mice in terms of β-diversity ($P = 0.001$; Fig. 6a,b). Potentially pathogenic bacteria including *L. bacterium* CAG:364, *L. bacterium* UBA7098, *P. bacterium* UBA7221 and *Alistipes* sp. *Marseille* P5061 were enriched in G-*Tm6sf2*$^{\Delta IEC}$ mice (Fig. 6c), of which the abundances of all these species were also increased in the donor *Tm6sf2*$^{\Delta IEC}$ mice (Fig. 2h). Protective Ruminococcaceae was depleted in G-*Tm6sf2*$^{\Delta IEC}$ mice (Fig. 6c). Moreover, untargeted and targeted metabolomics identified increased LPA levels in stools and portal vein serum of G-*Tm6sf2*$^{\Delta IEC}$ mice, compared to G-*Tm6sf2*^{fl} control mice (Fig. 6d–f). Correlation analysis further showed that the abundances of Porphyromonadaceae, Lachnospiraceae and *Alistipes* were positively correlated with LPA level, in contrast to Ruminococcaceae, which had a negative correlation (Fig. 6g). These results from FMT-treated germ-free mice thus confirm the significance of gut microbiota in mediating MASH development induced by intestinal *Tm6sf2* deficiency.

Gut microbiota modulation improves MASH in *Tm6sf2*$^{\Delta IEC}$ mice

Given the importance of the gut microbiota, therapeutic potential of microbiota modulation against MASH was investigated by co-housing *Tm6sf2*$^{\Delta IEC}$ mice with *Tm6sf2*^{fl} wild-type mice for 4 months (Fig. 7a). Gut microbial dysbiosis was restored with significantly decreased *L. bacterium* and *Porphyromonadeceae bacterium* in *Tm6sf2*$^{\Delta IEC}$ mice after co-housing (Extended Data Fig. 8). Co-housed *Tm6sf2*$^{\Delta IEC}$ mice exhibited ameliorated steatohepatitis with reduced hepatic lipid accumulation, MASH activity score and pro-inflammatory cytokines TNF and IL-6 (Fig. 7b,c). The proportions of activated macrophages ($P = 0.0012$) and M1 pro-inflammatory macrophages ($P = 0.0011$) were also significantly decreased in co-housed *Tm6sf2*$^{\Delta IEC}$ mice (Fig. 7d). Moreover, the width of intestinal tight junctions was markedly reduced in co-housed *Tm6sf2*$^{\Delta IEC}$ mice ($P = 0.0026$; Fig. 7e), implying the improved integrity of the intestinal barrier. These results thus suggest that targeting the gut microbiota is effective against MASH induced by intestinal *Tm6sf2* deficiency.

Pharmacological inhibition of LPA receptor suppresses MASH

Since unrestrained translocation of the toxic metabolite LPA from the gut to liver is crucial for disease development, we hypothesized that LPAR, the receptor of LPA, could be a therapeutic target of MASH. *Tm6sf2*$^{\Delta IEC}$ mice were treated with LPAR antagonist AM095 for 6 weeks (Fig. 8a). LPAR blockade markedly reduced lipid accumulation, MASH activity score, hepatic triglyceride, and lipid peroxidation in *Tm6sf2*$^{\Delta IEC}$ mice, compared to vehicle *Tm6sf2*$^{\Delta IEC}$ control mice (Fig. 8b,c). We further examined the effect of LPAR antagonist AM095 or Brp-LPA in wild-type mice with methionine–choline-deficient (MCD) diet-induced MASH. AM095 treatment alleviated diet-induced lipid accumulation, MASH activity score and triglyceride content in mice (Fig. 8d–f), while Brp-LPA significantly reversed diet-induced MASH with reduced lipid accumulation, MASH activity score and triglyceride content (Fig. 8g–i). Similarly, AM095 reversed HFHC diet-induced triglyceride accumulation and serum ALT levels in wild-type mice (Extended Data Fig. 9a–c). Collectively, these findings indicate that LPAR blockade is a promising therapeutic approach against MASH.

Discussion

In this study, we demonstrated a crucial cross-talk between an intestinal gene and liver disease. TM6SF2 is predominantly expressed in human liver and intestines, whereas its loss-of-function variant is a well-known risk factor of MASH. Using multiple mouse models, our results illustrated the contribution of intestinal *Tm6sf2* deficiency to the development of MASH. Mechanistically, TM6SF2 binds with FABP5 to regulate fatty acids in IECs, yet its deletion leads to increased release of free fatty acids into the intestinal microenvironment, harming the integrity of the intestinal barrier and altering the gut microbiota (Fig. 8j). The dysbiotic microbiota then triggers the secretion of toxic metabolite LPA, which is more likely to enter the portal vein due to the impaired intestinal barrier. The translocated LPA eventually promotes MASH development after binding to its receptor LPAR in the liver.

Human gut and liver communicate bidirectionally via the gut–liver axis, starting from the intestinal barrier, portal vein circulation, biliary tract and liver as the terminal. Previous studies have reported the association of various intestinal factors with liver diseases in the context of the gut–liver axis. For example, activation of intestine-specific hypoxia-inducible factor 2α under obesity is a contributor of hepatic steatosis[20], whereas high-density lipoproteins derived from enterocytes could restrain liver injury through the portal vein circulation[21]. On the other hand, although the correlation between the TM6SF2 variant and MASH is well reported[22], the impact of intestinal TM6SF2 on this disease remains unclear. Given the high expression of TM6SF2 in human intestines[8], we speculated the potential role of intestinal TM6SF2 in MASH. Using different mouse models with intestinal *Tm6sf2* deficiency, our results clearly illustrate that intestinal *Tm6sf2* deficiency promoted MASH and fibrosis in mice, which in turn indicates the protective role of intestinal TM6SF2 against MASH development.

Intestinal barrier dysfunction is a prerequisite for MASH development[14], while gut microbial dysbiosis is an important cause of such dysregulation. Our previous study reported that the intestinal barrier is impaired in individuals with the *TM6SF2* loss-of-function variant[12]. Here, we showed that intestinal barrier integrity is markedly impaired in *Tm6sf2*$^{\Delta IEC}$ mice, concomitant with an altered gut microbiota. In particular, potentially pathogenic *P. bacterium*, *L. bacterium* and *Alistipes* sp. *Marseille* were significantly enriched in *Tm6sf2*$^{\Delta IEC}$ mice. Porphyromonadaceae is a pro-inflammatory bacteria enriched in individuals with MASH[23], and it could exacerbate steatohepatitis in mice with inflammasome deficiency-induced MASH[24,25]. Similarly, enriched Lachnospiraceae was reported in individuals with MASLD[18] while inducing MASLD development in germ-free mice[26]. *Alistipes* sp. *Marseille* is a potential pathogenic bacterium enriched in mice fed with a high-fat diet and is positively correlated with serum LPA level[27]. Through metabolomic profiling, LPA was identified as one of the top metabolites that were consistently elevated in stools, portal vein serum and liver tissues of *Tm6sf2*$^{\Delta IEC}$ mice. LPA is a bioactive phospholipid known to exhibit pro-tumorigenic effects by inducing inflammation, liver steatosis and insulin resistance[28]. Integrative analysis revealed a positive correlation between LPA level and faecal abundances of Lachnospiraceae, Porphyromonadaceae and *Alistipes*. Moreover, Lachnospiraceae harbours two enzymes involved in LPA production. Germ-free mouse experiments confirmed that Lachnospiraceae was involved in LPA biosynthesis, while gut LPA could be translocated into the liver through the impaired intestinal barrier and portal vein. Hence, a dysregulated gut–liver axis caused by intestinal *Tm6sf2* deficiency leads to gut microbial dysbiosis and unrestrained translocation of LPA into the liver, thereby promoting MASH development.

The underlying mechanisms of how intestinal *Tm6sf2* deficiency induces gut microbial dysbiosis and metabolite alterations were investigated. IECs isolated from *Tm6sf2*$^{\Delta IEC}$ mice tend to secrete more free fatty acids especially LCFAs. Increased LCFAs including arachidic acid and arachidonic acid results in impaired intestinal barrier, elevated LPA level and enriched pathogenic bacteria including Lachnospiraceae and Porphyromonadaceae in mice. Similarly to our results, a previous report showed that diets with high contents of linolenic acid, palmitic acid and arachidic acid could change the gut microbiota and villus morphology in mouse small intestine[29]. In general, fatty acids are first absorbed in the intestines through the lipid transporter CD36, and then transported intracellularly by various FABPs[30]. The binding between free fatty acids and FABPs is critical to reduce toxicity of fatty acids in cells[30]. In this study, we revealed the direct binding between TM6SF2 and FABP5, while overexpressing FABP5, could reverse the increased secretion of LCFAs induced by *Tm6sf2* deletion in IECs. Together, our findings indicate that the binding between TM6SF2 and FABP5 is abolished under TM6SF2 deletion, which in turn promotes the release of

LCFAs and other free fatty acids from TM6SF2-deficient IECs. These secreted free fatty acids then stimulate the gut microbiota to produce more toxic metabolites particularly LPA, subsequently accelerating MASH development.

The causative role of the gut microbiota in MASH induced by intestinal *Tm6sf2* deficiency was validated by FMT. Indeed, the faecal microbiota from *Tm6sf2*$^{\Delta IEC}$ mice directly promoted lipid accumulation and inflammation in recipient germ-free mice, thus implying that the gut microbiota altered by intestinal *Tm6sf2* deficiency is adequate to induce MASH development in mice. Numerous preclinical and clinical studies have reported the therapeutic potential of dietary intervention, probiotics or FMT to modulate the gut microbiota against MASH[31–34]. Given its crucial role, we hypothesized that modulating the gut microbiota or their metabolites may be effective to ameliorate MASH. By co-housing *Tm6sf2*$^{\Delta IEC}$ mice with wild-type controls, the dysbiotic microbiota of *Tm6sf2*$^{\Delta IEC}$ mice was restored with ameliorated steatohepatitis. Besides, many antagonists of LPAR have been investigated in clinical trials as therapeutic targets for different pathologies[35]. In line with these studies, here we found that pharmacological blockade of LPAR also suppressed MASH in both *Tm6sf2*$^{\Delta IEC}$ mice and wild-type mice with diet-induced MASH. Collectively, while MASH is infamous for having very limited treatment options with only one drug approved by the US Food and Drug Administration, therapeutic potential of gut microbiota or metabolite manipulation against this disease is increasingly demonstrated.

This study has several limitations. Firstly, the findings are predominantly based on mouse models. Human studies are necessary to validate the significance of intestinal *Tm6sf2* in the progression of MASLD. Secondly, the evaluation of LPAR antagonist Brp-LPA was confined to an MCD mouse model, which inadequately recapitulates key metabolic risk factors necessary to represent the clinical spectrum of MASLD[36]. Nonetheless, although the MCD model is a nutrient-deficient approach that cannot accurately reflect the natural history of MASLD, it remains widely used in research due to its ability to induce severe inflammation and moderate hepatic fibrosis in a relatively short feeding period. Moreover, our investigation into the LPAR antagonist AM095 in mice with HFHC diet-induced MASH may address the limitation of the MCD mouse model.

In conclusion, our study reveals that deficiency of intestinal TM6SF2 is associated with MASH development. The loss of TM6SF2 promotes the release of free fatty acids from IECs, leading to intestinal barrier dysfunction, gut microbiota dysbiosis and metabolite alterations. These changes prompt the translocation of endotoxins and harmful metabolites into the liver, eventually accelerating MASH development. On the other hand, modulating the gut microbiota and their metabolites is effective in alleviating MASH in mice. Altogether, our findings report a gut–liver cross-talk in the development of liver disease, involving an intestinal gene, gut microbiota and metabolites, while targeting the microbiota or blocking metabolite receptors might be a potential strategy in the prevention and treatment of MASH induced by the TM6SF2 loss-of-function variant.

Methods

Mouse experiments

All animal experiments were performed in accordance with guidelines approved by the Animal Experimentation Ethics Committee of The Chinese University of Hong Kong, Xiamen University, Army Medical University and Gnotobio. Mice were housed in specific pathogen-free facilities at 20–26 °C with 40–70% humidity under a 12-h light–dark cycle. Food and water were provided ad libitum. Both male and female *Tm6sf2*$^{\Delta IEC}$ mice were used to investigate the role of intestinal *Tm6sf2* deficiency in steatohepatitis. For other experiments, male mice were used following the precedent set by prior MASLD studies that predominantly used male mice. No statistical methods were used to predetermine sample size. Mice were randomly assigned to each group.

Tm6sf2 transgenic mice. Conditional *Tm6sf2* KO C57BL/6J mice were generated through the Cre-loxP recombination system by Nanjing Biomedical Research Institute of Nanjing University (Extended Data Fig. 10a). *Tm6sf2*^{fl} mice were first generated by CRISPR–Cas9-targeted insertion of LoxP recombination sites into intronic regions that surround exons 2–5. The single-guide RNA (sgRNA) sequences are: 5′-AGGGGAATCCACCTGTC; 3′-CCCAACACTCAACCCCCG. These *Tm6sf2*^{fl} mice (3–4 weeks) were then cross-bred with Cre transgenic mice by in vitro fertilization to yield Cre/*Tm6sf2*^{loxP} mice. *Tm6sf2* was inactivated due to the deletion of exons 2–5, induced by Cre-loxP recombination. Tissue specificity of conditional *Tm6sf2* KO was contingent upon tissue-specific expression of the Cre recombinase. Alb-Cre (B6.Cg- Tg (Alb-Cre) 21 Mgn/JNju mice, Nanjing University) or Villin-Cre mice (B6.Cg-Tg(Vil1-cre)997Gum/J mice, RRID: IMSR_JAX:004586, The Jackson Laboratory) were used for liver-specific or IEC-specific *Tm6sf2* KO, respectively. Only homozygous conditional *Tm6sf2* KO mice were used for animal experiments.

Systemic *Tm6sf2* KO C57BL/6 mice were generated through the CRISPR–Cas9 system at the animal centre of Xiamen University, Xiamen, China. CRISPR–Cas9-mediated gene editing led to a four-base-pair deletion in the first exon of the *Tm6sf2* gene, causing a frameshift mutation that effectively inactivated *Tm6sf2* (Extended Data Fig. 10b). Backcross breeding with offsprings of C57BL/6 wild-type mice for three generations was used to remove any possible off-target changes. Genotyping was screened with primers listed in Supplementary Table 2. Sanger sequencing was performed on PCR products for verification.

Male *Tm6sf2*$^{\Delta Liver}$, *Tm6sf2*$^{\Delta IEC}$, *Tm6sf2* KO and their corresponding wild-type littermates (n = 5–12 per group) were fed with NC (13.38% fat, 57.94% carbohydrate, 28.67% protein; 5001, LabDiet) for 4 or 12 months, CD-HFD (36.2% fat, 27.3% carbohydrate, 27.2% protein; D19042402, Research Diets) for 2 or 14 months, or HFHC diet (43.7% fat, 36.6% carbohydrate, 19.7% protein; SF11-078, Specialty Feeds) for 2 months. Female *Tm6sf2*$^{\Delta IEC}$ and control mice (n = 9 per group) were fed with NC for 12 months. In additional experiments, 8-month-old NC-fed *Tm6sf2*$^{\Delta IEC}$ mice (n = 5 per group) were co-housed with *Tm6sf2*^{fl} littermates for 4 months. 12-month-old NC-fed *Tm6sf2*$^{\Delta IEC}$ mice (n = 5 per group) were injected with AM095 (10 mg per kg body weight) or vehicle control (10% DMSO) intraperitoneally twice per week for 6 weeks. Mice were fasted for 16 h before euthanasia.

Germ-free mice. Male C57BL/6 germ-free mice were bred in the Department of Laboratory Animal Services, Army Medical University, Chongqing, China. One gram of faecal samples from *Tm6sf2*$^{\Delta IEC}$ or *Tm6sf2*^{fl} mice was homogenized in 5 ml of PBS. Germ-free mice at 7 weeks old (n = 10–11 per group) were gavaged with faecal samples once at 2 months old and 3 months old, respectively. Mice were euthanized 4 months or 8 months after the first FMT.

Another batch of male C57BL/6 germ-free mice was acquired from Gnotobio. *L. bacterium* CAG364 (DSM 20583, German Collection of Microorganisms and Cell Cultures) were cultured under anaerobic conditions using DSMZ Medium 104. Germ-free mice (n = 5 per group) received a daily dose of 1×10^8 colony-forming units of *L. bacterium* for a consecutive period of 10 days.

Mice treated with free fatty acids. Male 7-week-old C57BL/6 mice (n = 5 per group) were fed with NC mixed with free fatty acids, including arachidic acid (10 g per kg body weight diet; A3631, Sigma-Aldrich), arachidonic acid (10 g per kg body weight diet; A3611, Sigma-Aldrich), linoleic acid (50 g per kg body weight diet; L1376, Sigma-Aldrich) and palmitic acid (22 g per kg body weight diet; P0500, Sigma-Aldrich) for 10 days. FITC–dextran assay was performed before euthanasia to determine intestinal permeability.

Mice treated with LPAR antagonists. Seven-week-old male C57BL/6 mice were fed with MCD diet (sucrose, 455.3 g per kg body weight; corn starch, 200 g per kg body weight; corn oil, 100 g per kg body

weight; 0296043910, MP Biomedicals) or corresponding control diet (sucrose, 455.3 g per kg body weight; corn starch, 200 g per kg body weight; corn oil, 100 g per kg body weight; choline chloride, 2 g per kg body weight; DL-methionine, 3 g per kg body weight, 0296044110, MP Biomedicals) for 10 days. AM095 (10 mg per kg body weight body weight; Apexbio) or vehicle control (10% DMSO) was intraperitoneally injected into mice (n = 5–8 per group) for a total of three times (days 3, 6 and 9). Male 7-week-old C57BL/6 mice were fed with a HFHC diet for 3 months and intraperitoneally injected with AM095 (30 mg per kg body weight) three times per week for another 1 month (n = 9–10 per group). To evaluate the effect of LPAR inhibition, male 7-week-old C57BL/6 mice were fed with an MCD diet for 2 weeks. Brp-LPA (7.5 mg per kg body weight; Echelon) or vehicle control (10% DMSO) was intraperitoneally injected into mice for three times (n = 5–6 per group) every 2 days for 1 week.

Cell culture and treatment

Mouse normal hepatocytes AML-12 cells (RRID: CVCL_0140, CRL-2254), human normal hepatocytes THLE-2 (RRID: CVCL_3803, CRL-2706), human colon epithelial cells Caco2 (RRID: CVCL_0025, HTB-37) and human HEK293T cells (RRID: CVCL_0063, CRL-3216) were purchased from the American Type Culture Collection. AML-12 cells were cultured in DMEM/F-12 medium (Gibco) supplemented with 10% FBS (Thermo Fisher Scientific), 5 mg ml^{-1} insulin, 5 µg ml^{-1} transferrin, 5 ng ml^{-1} selenium, 40 ng ml^{-1} dexamethasone and 1% penicillin–streptomycin (Thermo Fisher Scientific). Caco2 and HEK293T cells were cultured in DMEM supplemented with 10% FBS and 1% penicillin–streptomycin. THLE-2 cells were cultured in THLE-2 specific medium (CM-0833, Procell). Cells were maintained at 37 °C in a humidified incubator with 5% CO_2. Cells were serum starved for 24 h and maintained in medium containing 0.1% fatty acid-free BSA with or without supplementing 0.5 µM LPA for 48 h. For LPAR inhibition treatment, 10 µM AM095 was treated with cells for 1 h before LPA treatments. All cell lines were authenticated by short tandem repeat profiling, and tested immediately for *Mycoplasma* upon receipt using MycoAlert Mycoplasma Detection Kit (LT07-318, Lonza Bioscience).

Lentivirus production

sgRNAs for *TM6SF2* were designed by Hanyin Biotechnology (Shanghai) and cloned into CMV-MCS-3XFlag-PGK-Puro lentiviral vector. FABP5 plasmid was designed by Inovogen Technology and cloned into pLV-FABP5-Bsd lentiviral vector. sgRNAs were designed as follows: sgRNA for *TM6SF2*, FATTGATGAGCGCCCTAATCC; sgRNA for *FABP5*, TGGGAGGTCTATATAAGCAGAG. Lentiviral sgRNA vector was co-transfected into HEK293T cells with psPAX2 (12260, Addgene), pMD2.G (12259, Addgene) and Lipofectamine 2000 (Thermo Fisher Scientific) to produce lentivirus. Forty-eight hours after transfection, virus was collected and frozen at −80 °C.

Caco2 cells with TM6SF2 KO were generated through 48 h of lentiviral transduction, followed by puromycin selection. Caco2 cells with FABP5 overexpression were generated through 48 h of lentiviral transduction, followed by blasticidin HCl selection. Caco2 cells with both TM6SF2 KO and FABP5 overexpression were generated sequentially, first with TM6SF2 KO followed by FABP5 overexpression.

Primary small intestinal cell isolation

Small intestine tissues from *Tm6sf2*$^{\Delta IEC}$ and corresponding *Tm6sf2*^{fl} control mice were cut into small pieces (1–2 mm^3) and digested in 0.625 mg ml^{-1} collagenase IV, 0.125 mg ml^{-1} Dispase and antibiotics (50 µg ml^{-1} gentamicin, 5 µg ml^{-1} vancomycin and 0.5 µg ml^{-1} amphotericin B) for 1 h in a 37 °C shaker. The tissue suspension was then supplemented with 5 ml of DPBS with 10% FBS and filtered through a 70-µm cell strainer. The cell population was centrifuged at 400g for 5 min twice. Cell pellets were cultured in DMEM medium as primary IECs. Cell cultural medium was collected for metabolomic profiling.

Histological analysis

Liver histology was assessed by H&E staining of paraffin-embedded sections (4 µm). Histological scoring was independently evaluated by two investigators who were blinded to the group information. Steatosis and inflammation were scored as previously described[10]. MASH activity score was calculated by the sum of steatosis, inflammation and ballooning. The presence of steatosis was confirmed by Oil Red O staining of frozen sections. Oil Red O-positive areas were quantified by Image J (version 1.53e).

Transcriptomic sequencing

Total RNA was isolated from liver tissues of *Tm6sf2*$^{\Delta IEC}$ and *Tm6sf2*^{fl} mice by TRIzol Reagent (Thermo Fisher Scientific) according to the manufacturer's instructions, and subjected to transcriptomic sequencing (Illumina NovaSeq 6000 Sequencing System). TruSeq RNA Sample Preparation Kit (Illumina) was used for the construction of the sequencing library. Data were presented as reads per kilobase of exon per million reads mapped. Sequencing reads were preceded by removing adaptors using cutadapt (version 1.18) and mapped on the reference human genome (GENCODE version 30) by HISAT2 (version 2.1.0) with the default options. Differentially expressed genes (P < 0.05) were included in pathway and function analysis using clusterProfiler (v4.0)[37] based on Gene Ontology and KEGG pathway databases.

Shotgun metagenomic sequencing

Genomic DNA was extracted from 100 mg of mouse faecal samples using PowerSoil Pro Kit (Qiagen), and subjected to shotgun metagenomic sequencing (Illumina HiSeq 2000). Raw reads were checked using KneadData (v0.12.0, https://huttenhower.sph.harvard.edu/kneaddata/) to ensure that data consisted of high-quality microbial reads free from contaminants. Low-quality reads were removed using Trimmomatic (v0.36) with the option 'SLIDINGWINDOW:4:20 MINLEN:70 LEADING: 3 TRAILING: 3'. All adaptor sequences in paired-end reads were clipped based on universal Illumina Nextera and TruSeq adaptor sequences. The remaining reads were mapped to the mammalian genomes (hg38, felCat8, canFam3, mm10, rn6, susScr3, galGal4 and bosTau8, UCSC Genome Browser), 6,093 UNiVec sequences, 7,681 complete plastomes and 46,775 bacterial plasmids (National Center for Biotechnology Information (NCBI) RefSeq database) to remove potential habitat/laboratory-associated or extrachromosomal sequence contaminants after alignment using Bowtie2 (v2.4.5). Taxonomy was assigned to metagenomic clean reads using k-mer-based algorithms implemented in Kraken2 taxonomic annotation pipeline. A standard database comprising 13,844 bacterial genomes from the NCBI (http://www.ncbi.nlm.nih.gov/) was built by counting distinct 31-mers in the reference libraries using Jellyfish (v.2.3.0)[38]. Each k-mer in a read was mapped to the lowest common ancestor of all reference genomes with the exact k-mer matches. Each query was then classified into a taxon with the highest total hits of k-mer matched by pruning the general taxonomic trees affiliated with the mapped genomes. Bracken (v2.5.0) was used to accurately estimate taxonomic abundance at genus and species levels. The final metagenomic read counts were normalized by the cumulative sum scaling method using the microbiome R/Bioconductor package (https://github.com/microbiome/microbiome/)[38]. For analyses of α- and β-diversities, abundance variation analysis and data visualization, R packages phyloseq (v3.16; http://microbiome.github.com/micro-biome/), ggpubr (v0.6.0; https://rpkgs.datanovia.com/ggpubr/) and ComplexHeatmap (https://github.com/jokergoo/ComplexHeatmap/) were used.

The reference genomes were downloaded based on the Genome Taxonomy Database (R207). All genes in genomes were predicted by prodigal (v2.6.3) and annotated by emapper (v2.1.9) under the EggNOG (v5.0.2) and Biocyc (https://biocyc.org/) databases.

Untargeted and targeted metabolomics

Untargeted liquid chromatography with tandem mass spectrometry (MS/MS) was performed on stool (25 mg), portal vein serum (100 µl) and liver tissues (25 mg) using an Orbitrap Exploris 120 Mass Spectrometer (Orbitrap MS, Thermo Fisher Scientific) in Biotree (Shanghai). The mobile phase consisted of 25 mM NH_4OAc and 25 mM NH_4OH in water (pH 9.75). A TripleTOF mass spectrometer was used to acquire MS/MS spectra on an information-dependent mode with acquisition software (Analyst TF 1.7, AB Sciex). In each cycle, 12 precursor ions with intensity greater than 100 were chosen for fragmentation at a collision energy of 30 V (15 MS/MS events with a product ion accumulation time of 50 ms each).

Targeted metabolomic profiling of LPA was performed on liver tissues and portal vein sera of mice. Fifty microlitres of portal vein serum was mixed with 200 µl of extraction buffer (methanol:acetonitrile ratio of 1:1 + 0.1% formic acid, containing 1 ppm of internal standard (4-Cl-Phe)). Next, 10–20 mg of liver tissues was mixed with 500 µl of extraction buffer (acetonitrile:methanol:water ratio of 4:4:2 + 0.1% formic acid, containing 1 ppm of internal standard (4-Cl-Phe)). Samples were homogenized by ultrasonication in ice water for 15 min, following by centrifugation at 20,000*g* for 10 min to collect the supernatants and vacuum drying. The dried samples were then reconstituted in 100 µl of 50% methanol. Targeted metabolomic profiling of free fatty acids was performed in the cultural medium of primary intestinal cells and Caco2 cells. Metabolomic profiling was performed using a 6500+ Liquid chromatography/Electrospray Ionization - QTrap Mass Spectrometer (SCIEX).

In vivo and in vitro FITC–dextran assay

For the in vivo permeability test, mice were orally gavaged with 200 µl of 4 kDa FITC–dextran (600 mg per kg body weight; Sigma-Aldrich) after 4 h of fasting. Blood was collected 4 h after gavage and fivefold diluted with PBS. Serum concentration of FITC–dextran was measured at an excitation wavelength of 490 nm and an emission wavelength of 530 nm by fluorescence spectrometry. Serially diluted FITC–dextran was used to establish a standard curve.

For in vitro permeability test, Caco2 cells were seeded in Transwell for 21 days to differentiate into intestinal epithelium. Cells were then starved overnight and treated with 200 µM arachidic acid, 100 µM arachidonic acid or vehicle control (0.1% ethanol or 1% BSA). The permeability of cell monolayer was accessed by adding 500 µl of FITC–dextran (1 mg ml^{-1} in Hanks' Balanced Salt Solution (HBSS)) to the apical chamber. FITC–dextran concentration was measured after 2 h of incubation.

Tm6sf2 immunohistochemistry staining

Mouse liver and small intestine sections (4 µm) were mounted onto silane-coated glass slides. Anti-Tm6sf2 antibodies were kindly provided by H. Hobbs in Howard Hughes Medical Institute of University of Texas Southwestern Medical Center (TM6SF2 9E9, dilution 1:200) or from FabGennix (201AP, dilution 1:200). Haematoxylin was used for counterstaining and rabbit serum diluted to the same concentration of primary antibody was used as a negative control. Each random field was scored to the amount and intensity of positive staining as follows: 0 = no staining, 1 = positive in less than 33% of cells, 2 = positive in 33–66% of cells, and 3 = positive in more than 66% of cells.

Biochemical assays

ALT, aspartate aminotransferase and cholesterol levels in serum and culture medium were measured using Catalyst One Chemistry Analyzer (IDEXX Laboratories) according to the manufacturer's instructions. Triglyceride in liver and small intestine was detected using Wako E-test Triglyceride Kit (Wako Pure Chemical Industries). Lipid peroxidation was quantified by measuring malondialdehyde through a thiobarbituric acid-reactive substances assay (Sigma-Aldrich).

Determination of liver collagen content

Sirius Red staining for collagen was performed in paraffin-embedded liver sections with quantitative morphometric measurement. Hepatic hydroxyproline was measured using Hydroxyproline Assay Kit (Jiancheng Bioengineering) according to the manufacturer's instructions. In brief, liver tissues (80–100 mg) were homogenized in alkaline hydrolysis buffer at 95 °C for 10 min. Hydroxyproline level was measured at a wavelength of 550 nm.

Immunofluorescence staining

OCT-embedded frozen sections of liver and small intestine tissues were fixed in ice-cold acetone, washed with PBS and blocked with 1% BSA and avidin/biotin blocking agent. Sections were incubated with primary antibodies, including E-cadherin (14472, Cell Signaling Technology) and villin (NBP1-32841, Novus Biologicals) overnight at 4 °C. Slides were then incubated with fluorochrome-conjugated secondary antibodies and examined by confocal microscopy (TCS SP8, Leica).

Western blot

Protein from 30–50 mg tissues or cell lysis was extracted using Cyto-Buster Protein Extraction Reagent (Merck Millipore). Protein concentration was measured using Detergent Compatible Protein Assay (5000111, Bio-Rad). Around 20–40 mg of protein was separated by SDS–PAGE gel electrophoresis and transferred onto polyvinylidene difluoride membranes (GE Healthcare). Membranes were blocked and incubated with respective primary antibodies including TM6SF2 (H. Hobbs in Howard Hughes Medical Institute of University of Texas Southwestern Medical Center; dilution 1:500), phospho-NF-κB p65 (Ser536; RRID: AB_331284, 3033S, Cell Signaling Technology; dilution 1:1,000), NF-κB p65 (RRID: AB_10859369, 8242S, Cell Signaling Technology; dilution 1:1,000), IκBα (RRID: AB_390781, 4814, Cell Signaling Technology; dilution 1:1,000), E-cadherin (RRID: AB_2728770, 14472, Cell Signaling Technology; dilution 1:1,000), occludin (RRID: AB_2934013, 91131, Cell Signaling Technology; dilution 1:1,000), claudin 3 (RRID: AB_2833313, AF0129, Affinity Biosciences; dilution 1:500), CD36 (RRID: AB_2716564, ab133625, Abcam; dilution 1:1,000) and NPC1L1 (RRID: AB_10976493, ab124801, Abcam; dilution 1:1,000) overnight at 4 °C and then with secondary antibodies at room temperature for 1 h. Proteins of interest were visualized using Clarity Western ECL Substrate (1705061, Bio-Rad). β-Actin and GAPDH was used as the housekeeping control.

Real-time quantitative PCR

Total RNA was extracted from mouse liver or small intestine tissues (50 mg) using TRIzol reagent (Invitrogen) according to the manufacturer's instructions. RNA concentration and quality were measured using a spectrophotometer, and 1,000 ng of the extracted RNA was reversely transcribed into complementary DNA using PrimeScript RT Reagent Kit with gDNA Eraser (RR047B; Takara). Real-time quantitative PCR was performed using TB Green Premix Ex Taq (Takara) in QuantStudio 7 Flex Real-Time PCR System (Thermo Fisher Scientific). Primers used are listed in Supplementary Table 2.

Transmission electron microscopy

Small intestine tissues were collected and fixed in 2.0% glutaraldehyde in 0.1 mol l^{-1} sodium cacodylate (Electron Microscopy Sciences). Ultrathin sections were prepared on a Reichert Ultracut E ultramicrotome. The ultrastructure of tissues was examined using a Philips CM100 transmission electron microscope.

LPS and LBP detection

LPS levels in portal vein serum and liver tissues were measured using Mouse LPS ELISA Kit (Cusabio) according to the manufacturer's instructions. LBP concentration was measured using Mouse LBP Detection Kit (Hycult Biotech).

FACS analysis
Freshly isolated liver tissues were gently chopped in warm HBSS containing collagenase IV and incubated at 37 °C for 15 min. The enzymatic reaction was immediately stopped by adding ice-cold HBSS. The tissue suspension was filtered with a 70-µm cell strainer and centrifuged at 500*g* for 10 min. Next, 8 ml of resuspended cells was added to 4 ml of 80% Percoll, centrifuged at 500*g* for 10 min, and resuspended immediately in FACS buffer. Cell populations were stained with APC/Cyanine 7 anti-mouse CD45 recombinant antibody (RRID: AB_2890720, 157618, QA17A26, BioLegend), PE anti-mouse F4/80 recombinant antibody (RRID: AB_2832546, 157303, QA17A29, BioLegend), PE/Cyanine 7 anti-mouse/human CD11b antibody (RRID: AB_312798, 101215, M1/70, BioLegend), PerCP/Cyanine 5.5 anti-mouse CD206 (MMR) antibody (RRID: AB_2561991, 141715, C068C2, BioLegend), APC anti-mouse CD11c antibodies (RRID: AB_313778, 117309, N418, BioLegend) and FBD Horizon Fixable Viability Stain 520 (RRID: AB_2869573, 564407, BD Bioscience). All stained cells were analysed by flow cytometry (BD FACSCelesta Flow Cytometer, BD Biosciences). The cell population was analysed using FlowJo (v10.4).

Pull-down assay
Mouse intestine tissues were lysed in RIPA buffer for co-immunoprecipitation. One milligram of tissue lysates was incubated with 2 µg of anti-Tm6sf2 antibody or normal rabbit IgG control overnight at 4 °C. The lysate–antibody mixture was then incubated with 20 µl of Protein A/G Mix Magnetic Beads (Merck Millipore) for 4 h at 4 °C. The eluted proteins were separated using SDS–PAGE gel, and then analysed through silver staining and liquid chromatography with mass spectrometry.

The protein mixture was also incubated overnight at 4 °C with either anti-TM6SF2 antibody or anti-FABP5 antibody (RRID: AB_2100341, 12348-1-AP, Proteintech). The protein–antibody complex was then captured by incubating with 50 µl of Protein A/G Plus Agarose Beads (20423) or Protein A/G Magnetic Beads (88802; Thermo Fisher Scientific). Beads were washed with PBS containing 0.05% Tween-20 to remove unbound proteins. Captured proteins were eluted by boiling and analysed by western blot.

MST assay
To measure the direct binding between TM6SF2 and FABP5, FABP5 in a gradient of concentrations was incubated with 0.2 µg µl^{-1} of pre-labelled recombinant TM6SF2 for 30 min at room temperature. For measurement, the incubated mixture was loaded into Monolith Capillaries (1,000 count; MO-K022, NanoTemper Technologies) and loaded onto a Monolith NT.115 Instrument (NanoTemper Technologies). A cap scan of all capillaries was performed and an MST experiment was conducted using auto LED/excitation power and medium MST power. Data were analysed using MO.Affinity Analysis Software (v2.3, NanoTemper Technologies).

Molecular docking analysis
The amino acid sequences of TM6SF2 (Q9BZW4) and FABP5 (Q01469) were retrieved from the UniProt database. The protein domains of TM6SF2 and FABP5 were retrieved from the RCSB Protein Data Bank database and selected for analysis. Molecular docking was calculated and processed by Gromacs software. Docking, analysis and visualization were conducted using GMX-MM-PBSA.

Statistical analysis
All results are shown as the mean ± standard deviation unless specified. Data distribution was assumed to be normal, but this was not formally tested. Data collection and analysis were not performed blind to the conditions of the experiments. Student's t-test or Mann–Whitney *U* test was used to compare the difference in numerical variables between two groups. One-way ANOVA was used for multiple-group comparison. Microbial abundance between groups was compared by general linear models based on multivariate association using the MaAsLin2 package in R[39]. Spearman's rank correlation coefficient was used for correlation analysis between microbial abundance and metabolites. Sample sizes were established by referring to previous studies using a comparable experimental setup and considering the assay's recognized level of variability. All statistical tests were performed and plotted using R language or GraphPad Prism (v8). Two-sided *P* values smaller than 0.05 were considered statistically significant.

Inclusion and ethics statement
All collaborators of this study have fulfilled the criteria for authorship required by Nature Portfolio journals have been included as authors, as their participation was essential for the design and implementation of the study. We confirm that the author list of this manuscript does not include any large language models.

Reporting summary
Further information on research design is available in the Nature Portfolio Reporting Summary linked to this article.

Data availability
All data are available in the main text, Extended Data or Supplementary Information. The raw data of metagenomic sequencing and RNA sequencing in this study are deposited in the NCBI public repository under accession PRJNA1135953. The raw data of metabolomics are deposited in MetaboLights under accession MTBLS11004. Source data are provided with this paper.

Code availability
All customized scripts used in this study have been uploaded to https://github.com/chuanfaliu/Intestinal_TM6SF2_deficient_mice_multiomics/.

References
1. Loomba, R., Friedman, S. L. & Shulman, G. I. Mechanisms and disease consequences of nonalcoholic fatty liver disease. *Cell* **184**, 2537–2564 (2021).
2. Yu, J., Shen, J., Sun, T. T., Zhang, X. & Wong, N. Obesity, insulin resistance, NASH and hepatocellular carcinoma. *Semin. Cancer Biol.* **23**, 483–491 (2013).
3. Eslam, M., Valenti, L. & Romeo, S. Genetics and epigenetics of NAFLD and NASH: clinical impact. *J. Hepatol.* **68**, 268–279 (2018).
4. Kozlitina, J. et al. Exome-wide association study identifies a TM6SF2 variant that confers susceptibility to nonalcoholic fatty liver disease. *Nat. Genet.* **46**, 352–356 (2014).
5. Mahdessian, H. et al. TM6SF2 is a regulator of liver fat metabolism influencing triglyceride secretion and hepatic lipid droplet content. *Proc. Natl Acad. Sci. USA* **111**, 8913–8918 (2014).
6. Fan, Y. et al. Hepatic transmembrane 6 superfamily member 2 regulates cholesterol metabolism in mice. *Gastroenterology* **150**, 1208–1218 (2016).
7. Newberry, E. P. et al. Liver-specific deletion of mouse Tm6sf2 promotes steatosis, fibrosis, and hepatocellular cancer. *Hepatology* **74**, 1203–1219 (2021).
8. Luo, F., Oldoni, F. & Das, A. TM6SF2: a novel genetic player in nonalcoholic fatty liver and cardiovascular disease. *Hepatol. Commun.* **6**, 448–460 (2022).
9. O'Hare, E. A. et al. TM6SF2 rs58542926 impacts lipid processing in liver and small intestine. *Hepatology* **65**, 1526–1542 (2017).
10. Zhang, X. et al. Dietary cholesterol drives fatty liver-associated liver cancer by modulating gut microbiota and metabolites. *Gut* **70**, 761–774 (2021).
11. Pan, Y. & Zhang, X. Diet and gut microbiome in fatty liver and its associated liver cancer. *J. Gastroenterol. Hepatol.* **37**, 7–14 (2022).

12. Pang, J. et al. Significant positive association of endotoxemia with histological severity in 237 patients with non-alcoholic fatty liver disease. *Aliment. Pharmacol. Ther.* **46**, 175–182 (2017).
13. Wu, R., Nakatsu, G., Zhang, X. & Yu, J. Pathophysiological mechanisms and therapeutic potentials of macrophages in non-alcoholic steatohepatitis. *Expert Opin. Ther. Targets* **20**, 615–626 (2016).
14. Mouries, J. et al. Microbiota-driven gut vascular barrier disruption is a prerequisite for non-alcoholic steatohepatitis development. *J. Hepatol.* **71**, 1216–1228 (2019).
15. Song, Q. & Zhang, X. The role of gut–liver axis in gut microbiome dysbiosis associated NAFLD and NAFLD-HCC. *Biomedicines* https://doi.org/10.3390/biomedicines10030524 (2022).
16. Liu, J. et al. Integrative metabolomic characterisation identifies altered portal vein serum metabolome contributing to human hepatocellular carcinoma. *Gut* **71**, 1203–1213 (2022).
17. Yang, W. et al. A distinct type of glycerol-3-phosphate acyltransferase with sn-2 preference and phosphatase activity producing 2-monoacylglycerol. *Proc. Natl Acad. Sci. USA* **107**, 12040–12045 (2010).
18. Shen, F. et al. Gut microbiota dysbiosis in patients with non-alcoholic fatty liver disease. *Hepatobiliary Pancreat. Dis. Int.* **16**, 375–381 (2017).
19. Yung, Y. C., Stoddard, N. C. & Chun, J. LPA receptor signaling: pharmacology, physiology, and pathophysiology. *J. Lipid Res.* **55**, 1192–1214 (2014).
20. Wu, Q. et al. Intestinal hypoxia-inducible factor 2alpha regulates lactate levels to shape the gut microbiome and alter thermogenesis. *Cell Metab.* **33**, 1988–2003 (2021).
21. Han, Y. H. et al. Enterically derived high-density lipoprotein restrains liver injury through the portal vein. *Science* https://doi.org/10.1126/science.abe6729 (2021).
22. Wong, V. W., Wong, G. L., Tse, C. H. & Chan, H. L. Prevalence of the *TM6SF2* variant and non-alcoholic fatty liver disease in Chinese. *J. Hepatol.* **61**, 708–709 (2014).
23. Wong, V. W. et al. Molecular characterization of the fecal microbiota in patients with nonalcoholic steatohepatitis—a longitudinal study. *PLoS ONE* **8**, e62885 (2013).
24. Garidou, L. et al. The gut microbiota regulates intestinal CD4 T cells expressing RORγt and controls metabolic disease. *Cell Metab.* **22**, 100–112 (2015).
25. Henao-Mejia, J. et al. Inflammasome-mediated dysbiosis regulates progression of NAFLD and obesity. *Nature* **482**, 179–185 (2012).
26. Kolodziejczyk, A. A., Zheng, D., Shibolet, O. & Elinav, E. The role of the microbiome in NAFLD and NASH. *EMBO Mol. Med.* https://doi.org/10.15252/emmm.201809302 (2019).
27. Yang, J. et al. High-fat diet promotes colorectal tumorigenesis through modulating gut microbiota and metabolites. *Gastroenterology* **162**, 135–149 (2022).
28. Kaffe, E., Magkrioti, C. & Aidinis, V. Deregulated lysophosphatidic acid metabolism and signaling in liver cancer. *Cancers* https://doi.org/10.3390/cancers11111626 (2019).
29. Todorov, H. et al. alpha-linolenic acid-rich diet influences microbiota composition and villus morphology of the mouse small intestine. *Nutrients* https://doi.org/10.3390/nu12030732 (2020).
30. Ko, C. W., Qu, J., Black, D. D. & Tso, P. Regulation of intestinal lipid metabolism: current concepts and relevance to disease. *Nat. Rev. Gastroenterol. Hepatol.* **17**, 169–183 (2020).
31. Wong, V. W. et al. Treatment of nonalcoholic steatohepatitis with probiotics. A proof-of-concept study. *Ann. Hepatol.* **12**, 256–262 (2013).
32. Zhou, D. et al. Total fecal microbiota transplantation alleviates high-fat diet-induced steatohepatitis in mice via beneficial regulation of gut microbiota. *Sci. Rep.* **7**, 1529 (2017).
33. Bomhof, M. R. et al. Histological improvement of non-alcoholic steatohepatitis with a prebiotic: a pilot clinical trial. *Eur. J. Nutr.* **58**, 1735–1745 (2019).
34. Wei, W. et al. Parabacteroides distasonis uses dietary inulin to suppress NASH via its metabolite pentadecanoic acid. *Nat. Microbiol* **8**, 1534–1548 (2023).
35. Geraldo, L. H. M. et al. Role of lysophosphatidic acid and its receptors in health and disease: novel therapeutic strategies. *Signal Transduct. Target. Ther.* **6**, 45 (2021).
36. Hsu, C. L. & Loomba, R. From NAFLD to MASLD: implications of the new nomenclature for preclinical and clinical research. *Nat. Metab.* **6**, 600–602 (2024).
37. Wu, T. et al. clusterProfiler 4.0: a universal enrichment tool for interpreting omics data. *Innovation* **2**, 100141 (2021).
38. Paulson, J. N., Stine, O. C., Bravo, H. C. & Pop, M. Differential abundance analysis for microbial marker-gene surveys. *Nat. Methods* **10**, 1200–1202 (2013).
39. Mallick, H. et al. Multivariable association discovery in population-scale meta-omics studies. *PLoS Comput. Biol.* **17**, e1009442 (2021).

Acknowledgements

This work was supported by National Natural Science Foundation of China (82222901, 82103355 and 82272619; to X.Z.); Research Grants Council-General Research Fund (CUHK 14117422,CUHK 14117123 and CUHK 14119524; to X.Z.); Health and Medical Research Fund, Hong Kong (08191336, 07210097; to X.Z.); Innovation and Technology Fund-Guangdong-Hong Kong Technology Cooperation Funding Scheme (GHP/086/21GD; to J.Y.); RGC Theme-based Research Scheme (T12-703/19-R; to J.Y.); Strategic Seed Funding Collaboration Research Scheme CUHK (3133344; to J.Y.); Strategic Impact Enhancement Fund CUHK (3135509; to J.Y.); Impact case for RAE CUHK (3134277; to J.Y.); CUHK Research Startup Fund (FPU/2023/149). We acknowledge H. Hobbs from Howard Hughes Medical Institute of University of Texas Southwestern Medical Centre for providing TM6SF2 9E9 antibody.

Author contributions

X.Z. performed experiments, analysed the data and drafted the manuscript. H.C.-H.L. performed experiments and revised the manuscript. S.H., C. Liang, H.W.L., Q.W.-Y.N., Y.Z., F.J., Y.Z., Y.P., Y.S., Y.Z. and J.C.Y.L. performed experiments. C. Liu conducted bioinformatic analyses. A.H.K.C. performed the histological evaluation as a pathologist. J.W. and H.X. helped to construct the transgenic mice. X.L. and C.C.W. commented on the study. V.W.-S.W. designed the study and revised the manuscript. J.Y. designed and supervised the study and revised the manuscript.

Competing interests

The authors declare no competing interests.

Additional information

Extended data is available for this paper at https://doi.org/10.1038/s42255-024-01177-7.

Supplementary information The online version contains supplementary material available at https://doi.org/10.1038/s42255-024-01177-7.

Correspondence and requests for materials should be addressed to Vincent Wai-Sun Wong or Jun Yu.

Peer review information *Nature Metabolism* thanks Herbert Tilg and the other, anonymous, reviewer(s) for their contribution to the peer review of this work. Primary Handling Editor: Yanina-Yasmin Pesch, in collaboration with the *Nature Metabolism* team.

[1]Department of Medicine and Therapeutics, Institute of Digestive Disease, State Key Laboratory of Digestive Disease, Li Ka Shing Institute of Health Sciences, The Chinese University of Hong Kong, Hong Kong SAR, China. [2]Institute of Precision Medicine, First Affiliated Hospital, Sun Yat-sen University, Guangzhou, China. [3]Department of Internal Medicine, Institute of Gastroenterology, Yonsei University College of Medicine, Seoul, South Korea. [4]Department of Gastroenterology, Zhongshan Hospital, Xiamen University, Xiamen, China. [5]Department of Anatomical and Cellular Pathology, The Chinese University of Hong Kong, Hong Kong SAR, China. [6]State Key Laboratory of Cellular Stress Biology, School of Medicine, Xiamen University, Xiamen, China. ✉e-mail: wongv@cuhk.edu.hk; junyu@cuhk.edu.hk

https://doi.org/10.1038/s42255-024-01177-7

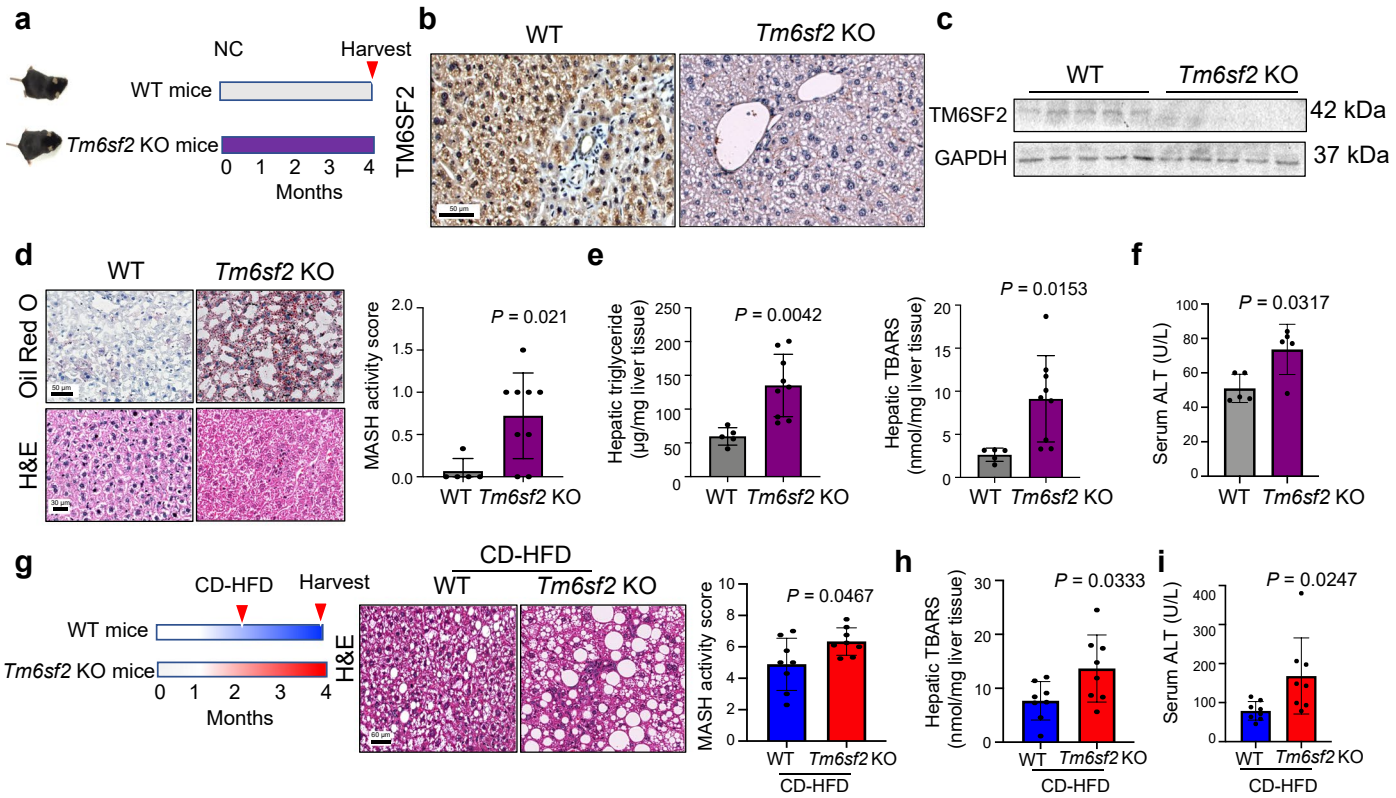

Extended Data Fig. 1 | Systemic *Tm6sf2* deficiency triggers MASH in mice. (**a**) Experimental schematic of systematic *Tm6sf2* KO and wildtype control mice fed with NC for 4 months; (**b, c**) Representative images of Tm6sf2 immunohistochemistry (**b**), and Tm6sf2 protein expression in liver tissues (**c**) of systematic *Tm6sf2* KO and wildtype mice ($n = 5$ per group); (**d-f**) Representative images of Oil Red O and H&E staining with histological scoring (**d**), hepatic triglyceride and lipid peroxidation (**e**), and serum ALT level (**f**) in *Tm6sf2* KO ($n = 9$) and wildtype mice ($n = 5$); (**g-i**) Experimental schematic and representative images of H&E staining with histological scoring (**g**), hepatic lipid peroxidation (**h**), and serum ALT level (**i**) of systematic *Tm6sf2* KO and wildtype control mice fed with CD-HFD for 2 months ($n = 8$ per group). Results are presented as mean ± s.d. Statistical significance was determined by two-tailed Student's t test (e, g-**i**) and Mann-Whitney U test (**d and f**).

https://doi.org/10.1038/s42255-024-01177-7

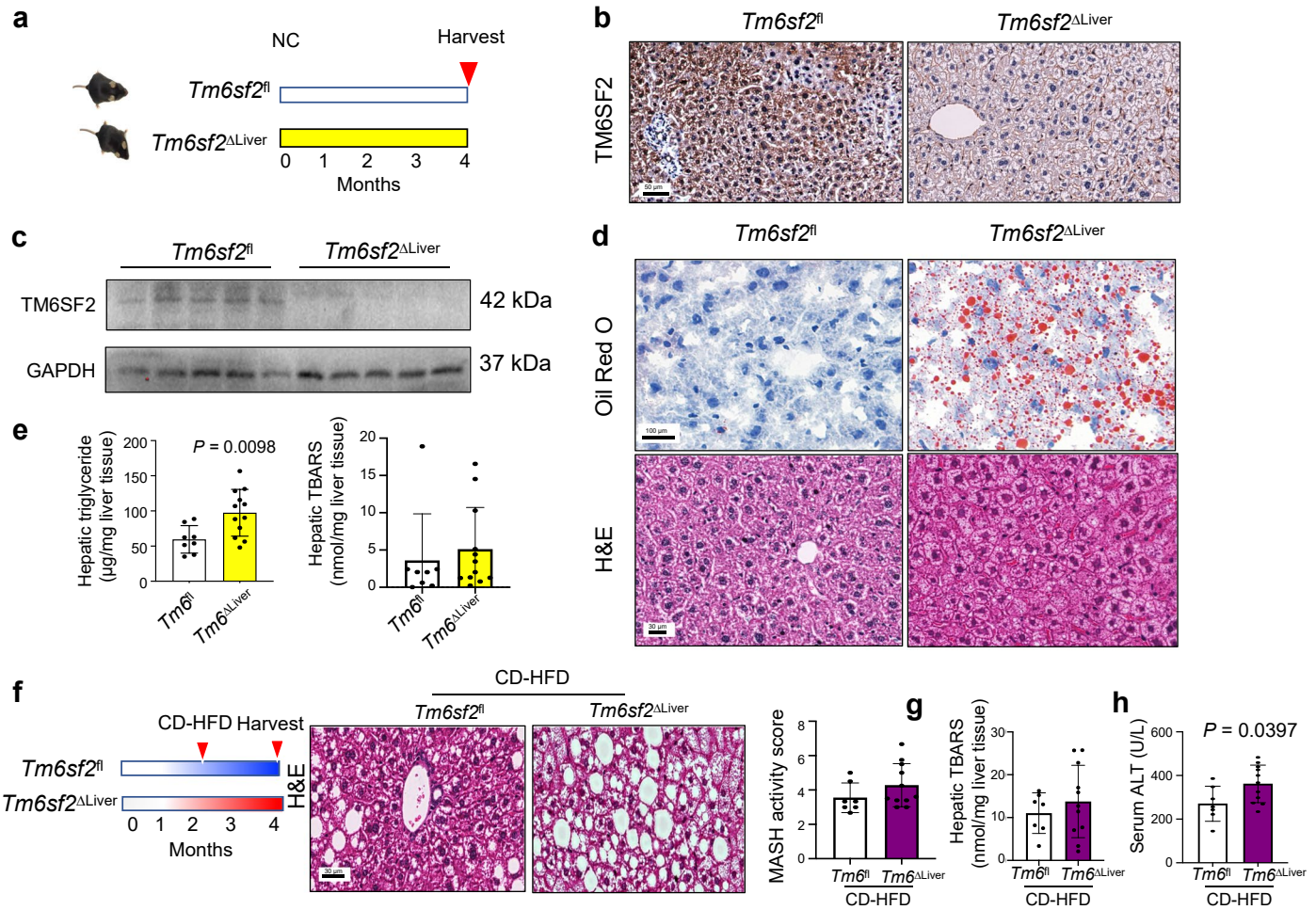

Extended Data Fig. 2 | Liver *Tm6sf2* deletion induces hepatic lipid accumulation in mice. (**a**) Experimental schematic of *Tm6sf2*$^{\Delta Liver}$ and *Tm6sf2*^{fl} mice fed with NC for 4 months; (**b-e**) Representative images of Tm6sf2 immunohistochemistry (**b**), hepatic Tm6sf2 protein expression (*n* = 5 per group) (**c**), representative images of Oil Red O and H&E staining with histological scoring (**d**), and hepatic triglyceride and lipid peroxidation (**e**) of *Tm6sf2*$^{\Delta Liver}$ (*n* = 12) and *Tm6sf2*^{fl} mice (*n* = 8); (**f-h**) Experimental schematic and representative images of H&E staining with histological scoring (**f**), hepatic lipid peroxidation (**g**), and serum ALT level (**h**) of *Tm6sf2*$^{\Delta Liver}$ (*n* = 11) and *Tm6sf2*^{fl} mice (*n* = 7) fed with CD-HFD for 2 months. Results are presented as mean ± s.d. Statistical significance was determined by two-tailed Student's t test (**e-h**).

https://doi.org/10.1038/s42255-024-01177-7

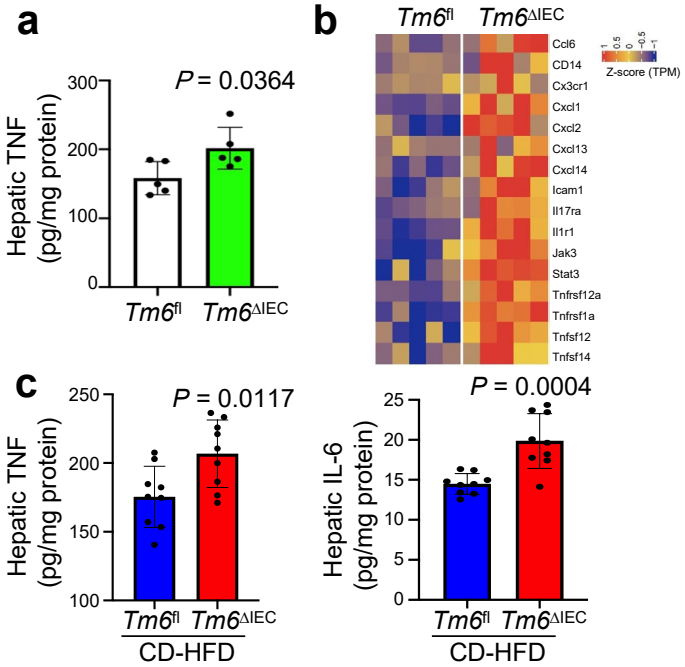

Extended Data Fig. 3 | Hepatic levels of pro-inflammatory cytokines in *Tm6sf2*$^{\Delta IEC}$ mice. (**a**, **b**) Hepatic TNF (**a**) and mRNA levels of pro-inflammatory cytokines (**b**) of NC-fed *Tm6sf2*$^{\Delta IEC}$ and *Tm6sf2*^{fl} mice at 12-month-old (n=5 per group); (**c**) Hepatic TNF and IL-6 levels of CD-HFD-fed *Tm6sf2*$^{\Delta IEC}$ and *Tm6sf2*^{fl} mice (n = 9 per group). Results are presented as mean ± s.d. Statistical significance was determined by two-tailed Student's t test (**a**-**c**).

https://doi.org/10.1038/s42255-024-01177-7

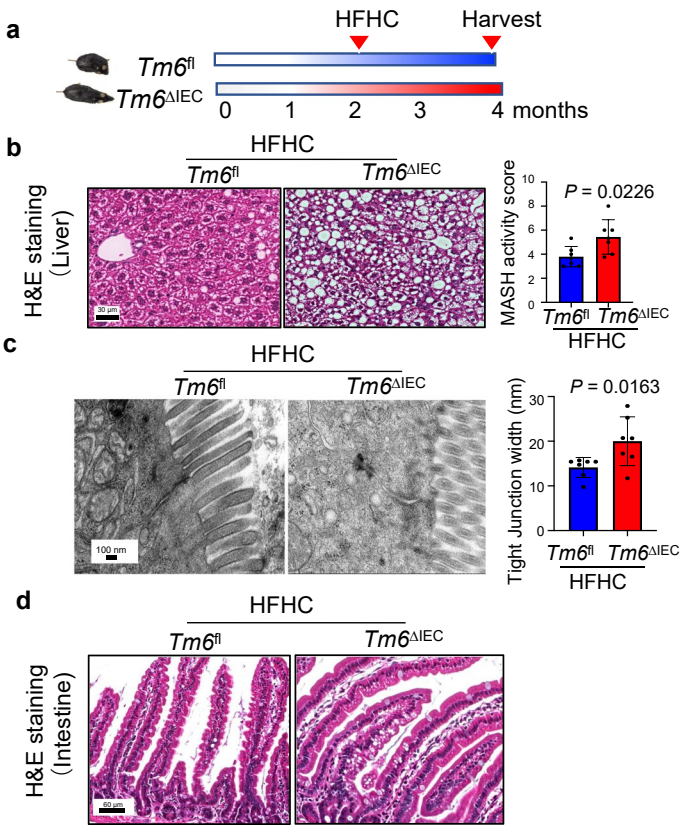

Extended Data Fig. 4 | Intestine *Tm6sf2* deficiency in mice accelerates HFHC diet-induced MASH. (**a**) Experimental schematic of *Tm6sf2*$^{\Delta IEC}$ and *Tm6sf2*^{flo} mice fed with HFHC diet; (**b**) Representative hepatic images of H&E staining with histological scoring of HFHC-fed *Tm6sf2*$^{\Delta IEC}$ and *Tm6sf2*^{flo} mice ($n = 7$ per group); (**c, d**) Representative small intestine images of transmission electron microscopy with tight junction width (**c**), and H&E staining (**d**) of HFHC-fed *Tm6sf2*$^{\Delta IEC}$ and *Tm6sf2*^{flox} mice ($n = 7$ per group). Results are presented as mean ± s.d. Statistical significance was determined by two-tailed Student's t test (**b**) and two-tailed Mann-Whitney *U* test (**c**).

https://doi.org/10.1038/s42255-024-01177-7

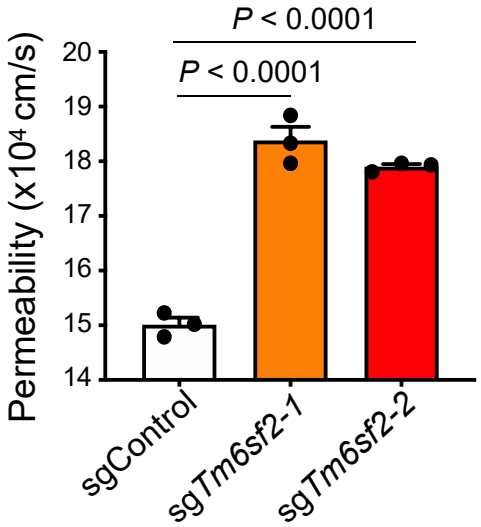

Extended Data Fig. 5 | *Tm6sf2* knockout increases intestinal epithelial cell permeability *in vitro*. Permeability of Caco2 cell monolayers treated with sgRNA-*Tm6sf2* ($n = 3$ per group). Results are presented as mean ± s.d. Statistical significance was determined by one-way ANOVA followed by Turkey's multiple comparison.

https://doi.org/10.1038/s42255-024-01177-7

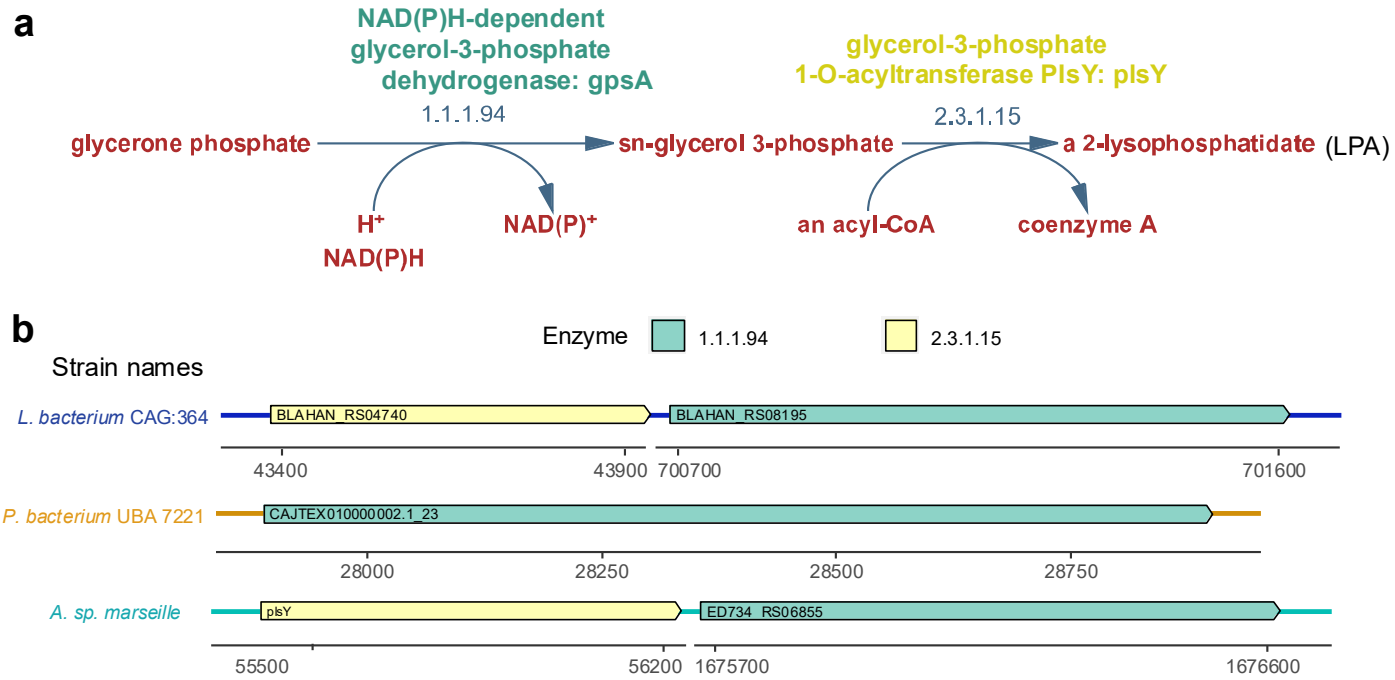

Extended Data Fig. 6 | Functional prediction of LPA-producing bacteria. (**a**) NAD(P)H-dependent glycerol-3-phosphate dehydrogenase [1.1.1.94] (gene: *gpsA*) and glycerol-3-phosphate 1-O-acyltransferase PlsY [2.3.1.15] (gene: *plsY*) are the key enzymes catalyzing glycerone phosphate to sn-glycerol 3-phosphate, the precursor of LPA; (**b**) Reference genomes of *P. bacterium* with genes encoding *gpsA*, and *L. bacterium* and *A. marseille* with genes encoding both *plsY* and *gpsA*.

https://doi.org/10.1038/s42255-024-01177-7

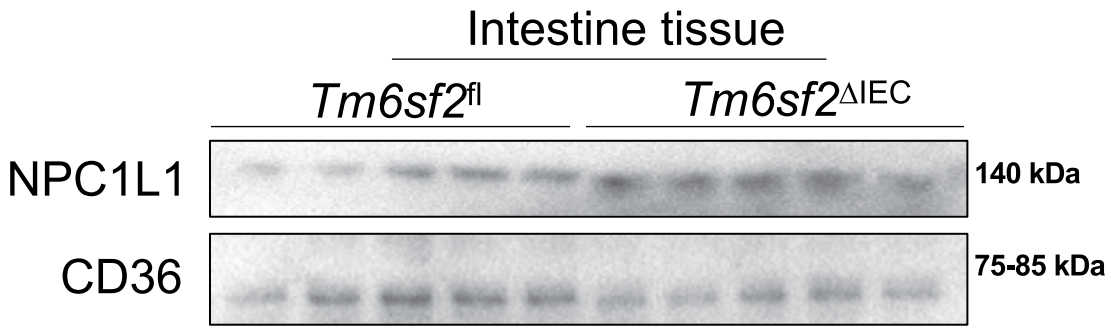

Extended Data Fig. 7 | Western blot analysis of NPC1L1 and CD36. NPC1L1 and CD36 protein expression in the small intestine of *Tm6sf2*$^{\Delta IEC}$ and *Tm6sf2*^{flox} mice ($n = 5$ per group). Housekeeping controls are identical to the left panel of Fig. 1c.

https://doi.org/10.1038/s42255-024-01177-7

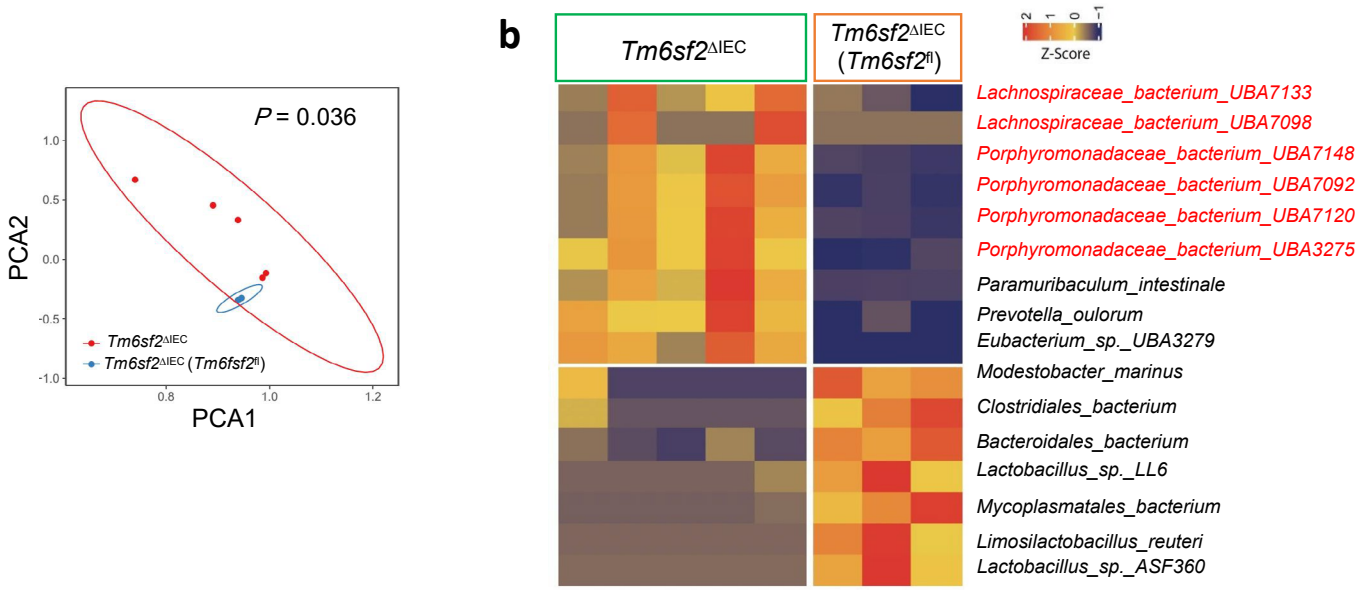

Extended Data Fig. 8 | Gut microbiota modulation by co-housing. (**a, b**) PCA analysis (**a**) and heatmap of differential fecal microbes (**b**) of *Tm6sf2*$^{\Delta IEC}$ ($n = 5$) and co-housed *Tm6sf2*$^{\Delta IEC}$ mice ($n = 3$). Statistical significance was determined by adonis (**a**).

https://doi.org/10.1038/s42255-024-01177-7

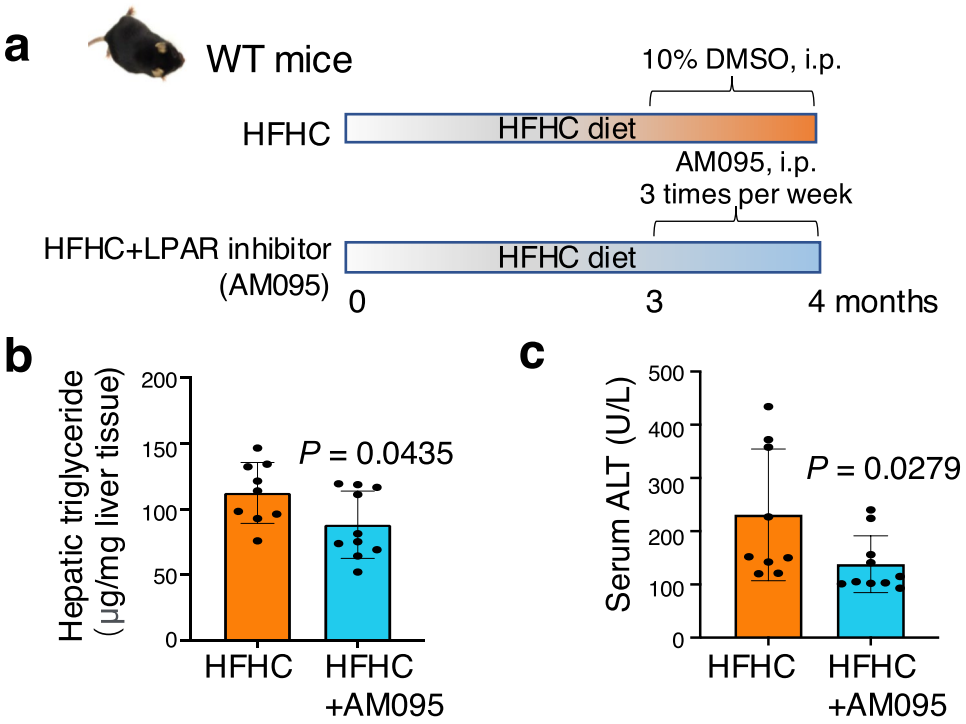

Extended Data Fig. 9 | LPAR inhibitor impairs HFHC diet-induced lipid accumulation and liver injury in mice. (**a-c**) Experimental schematic (**a**), hepatic triglyceride (**b**), and serum ALT level (**c**) of C57BL/6 wildtype mice fed with HFHC diet for 3 months and treated with vehicle control ($n = 9$) or LPAR inhibitor AM095 ($n = 10$) for 1 month. Results are presented as mean ± s.d. Statistical significance was determined by two-sided Mann-Whitney U test (**b, c**).

https://doi.org/10.1038/s42255-024-01177-7

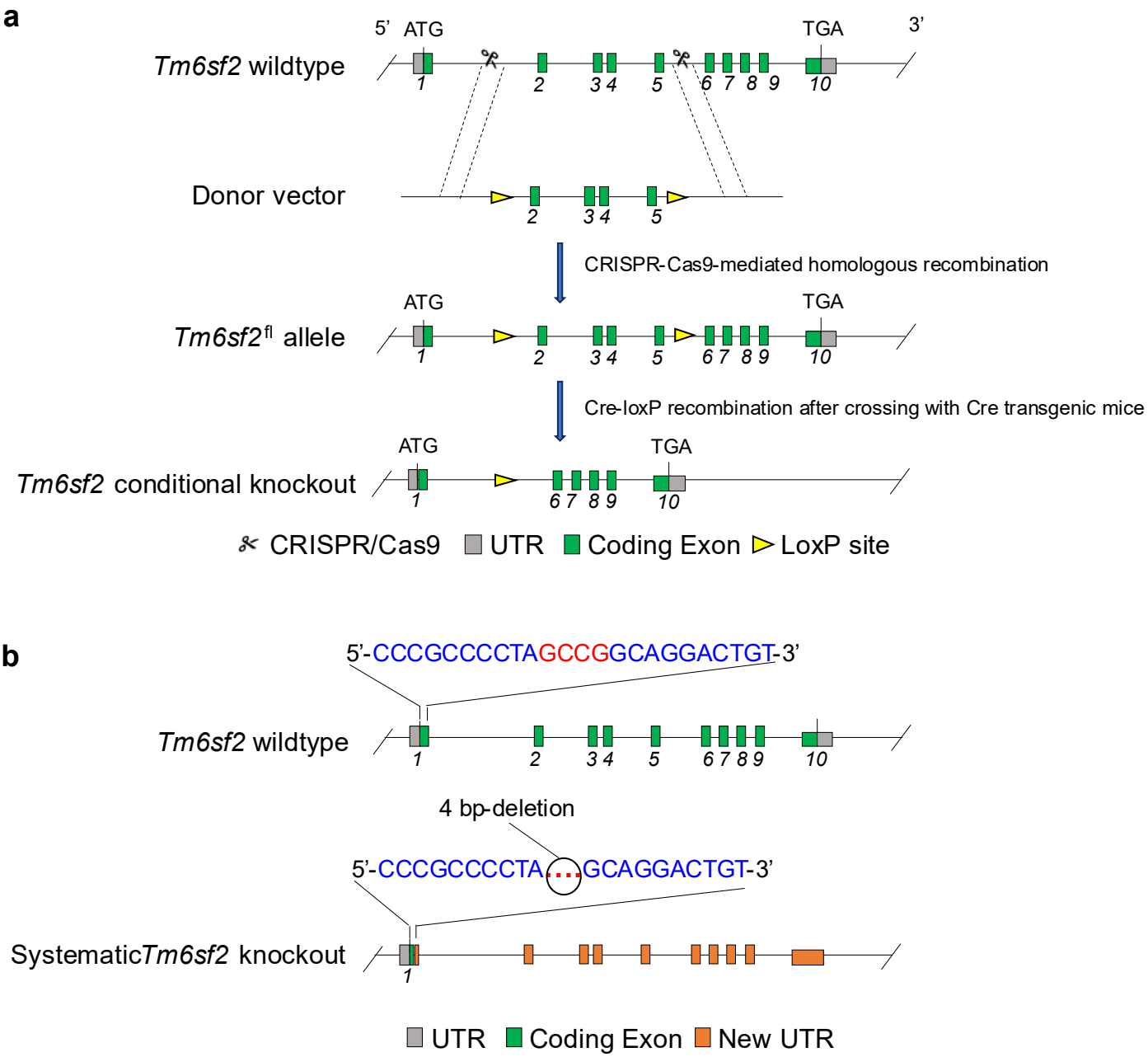

Extended Data Fig. 10 | Strategies for generating conditional *Tm6sf2* KO mice and systematic *Tm6sf2* KO mice. (**a**) Conditional *Tm6sf2* KO C57BL/6 mice were generated through targeted deletion of exons 2-5, induced by Cre-loxP recombination in tissue-specific manner; (**b**) Systematic *Tm6sf2* KO C57BL/6 mice were generated using CRISPR/Cas9 system by deleting a 4-base pair in the first exon of *Tm6sf2* gene.

nature portfolio

Corresponding author(s): Jun Yu

Last updated by author(s): Jan 5, 2025

Reporting Summary

Nature Portfolio wishes to improve the reproducibility of the work that we publish. This form provides structure for consistency and transparency in reporting. For further information on Nature Portfolio policies, see our Editorial Policies and the Editorial Policy Checklist.

Statistics

For all statistical analyses, confirm that the following items are present in the figure legend, table legend, main text, or Methods section.

n/a	Confirmed
☐	☒ The exact sample size (*n*) for each experimental group/condition, given as a discrete number and unit of measurement
☐	☒ A statement on whether measurements were taken from distinct samples or whether the same sample was measured repeatedly
☐	☒ The statistical test(s) used AND whether they are one- or two-sided *Only common tests should be described solely by name; describe more complex techniques in the Methods section.*
☒	☐ A description of all covariates tested
☒	☐ A description of any assumptions or corrections, such as tests of normality and adjustment for multiple comparisons
☐	☒ A full description of the statistical parameters including central tendency (e.g. means) or other basic estimates (e.g. regression coefficient) AND variation (e.g. standard deviation) or associated estimates of uncertainty (e.g. confidence intervals)
☐	☒ For null hypothesis testing, the test statistic (e.g. *F*, *t*, *r*) with confidence intervals, effect sizes, degrees of freedom and *P* value noted *Give P values as exact values whenever suitable.*
☒	☐ For Bayesian analysis, information on the choice of priors and Markov chain Monte Carlo settings
☒	☐ For hierarchical and complex designs, identification of the appropriate level for tests and full reporting of outcomes
☒	☐ Estimates of effect sizes (e.g. Cohen's *d*, Pearson's *r*), indicating how they were calculated

Our web collection on statistics for biologists contains articles on many of the points above.

Software and code

Policy information about availability of computer code

Data collection	Zeiss Imager Z2 Microscope equipped with automatic slide scanning feature (Zeiss, Oberkochen, Germany); Philips CM100 TEM (Philips/FEI Corporation, Eindhoven, Netherlands); confocal immunofluorescence microscopy (Leica SP8, Wetzlar, Germany); Analyst TF 1.7 (AB Sciex LLC, Framingham, MA); Illumina HiSeq 2000 platform (Illumina, San Diego, CA); Illumina NovaSeq 6000 Sequencing System (Illumina); Orbitrap Exploris™ 120 Mass Spectrometer (Thermo Scientific, Waltham, MA); 6500+ Liquid chromatography/Electrospray Ionization - QTrap Mass Spectrometer (SCIEX, Framingham, MA); BD FACSCelestaTM flow cytometry (Biosciences, San Jose, CA); Monolith NT.115 instrument (NanoTemper Technologies, Munich, Germany). All customized scripts used in this study have been uploaded to https://github.com/chuanfaliu/Intestinal_TM6SF2_deficient_mice_multiomics.
Data analysis	GraphPad Software v 8.0; R software v.3.5.2; Image J v. 1.53; Image Lab v 6.1; FlowJo software v10, KneadData v0.12.0; Trimmomatic v0.36; Bowtie2 v2.4.5; Bracken v2.5.0; prodigal v 2.6.3; emapper v 2.1.9; Gromacs software; MO. Affinity Analysis Software v2.3; microbiome R/Bioconductor package; phyloseq v3.16; ggpubr v0.6.0; eggnog DB v5.0.2; cutadapt v 1.18;HISAT2 v 2.1.0.

For manuscripts utilizing custom algorithms or software that are central to the research but not yet described in published literature, software must be made available to editors and reviewers. We strongly encourage code deposition in a community repository (e.g. GitHub). See the Nature Portfolio guidelines for submitting code & software for further information.

Data

Policy information about availability of data

All manuscripts must include a data availability statement. This statement should provide the following information, where applicable:

- Accession codes, unique identifiers, or web links for publicly available datasets
- A description of any restrictions on data availability
- For clinical datasets or third party data, please ensure that the statement adheres to our policy

All data are available in the main text, extended data or supplementary materials. The raw data of metagenomic sequencing and RNA sequencing in this study was deposited in the NCBI public repository under the accession number PRJNA1135953. The raw data of metabolomics was deposited in MetaboLights under accession number MTBLS11004.

Research involving human participants, their data, or biological material

Policy information about studies with human participants or human data. See also policy information about sex, gender (identity/presentation), and sexual orientation and race, ethnicity and racism.

Reporting on sex and gender	N/A
Reporting on race, ethnicity, or other socially relevant groupings	N/A
Population characteristics	N/A
Recruitment	N/A
Ethics oversight	N/A

Note that full information on the approval of the study protocol must also be provided in the manuscript.

Field-specific reporting

Please select the one below that is the best fit for your research. If you are not sure, read the appropriate sections before making your selection.

☒ Life sciences ☐ Behavioural & social sciences ☐ Ecological, evolutionary & environmental sciences

For a reference copy of the document with all sections, see nature.com/documents/nr-reporting-summary-flat.pdf

Life sciences study design

All studies must disclose on these points even when the disclosure is negative.

Sample size	Statistical methods were not employed to pre-determine the sample size, but sample sizes were determined by referencing our prior studies with similar experimental configurations (J Hepatol 2014, PMID:25048951; J Jepatol 2016, PMID: 26394162) and taking into account the well-recognized assay variability.
Data exclusions	Pre-established exclusion criteria were applied before conducting experiments, typically due to technical discrepancy or animals displaying abnormal conditions, such as mortality.
Replication	The reproducibility of the findings was verified in multiple mouse models and cell lines. Findings from mice and cell lines were replicated using at least 3 independent and biologically distinct samples.
Randomization	All samples and animals were allocated to each group randomly.
Blinding	The analyses for metagenomic sequencing, non-targeted metabolomics, transcriptome sequencing, and histological scores were conducted in a blinded manner. Other data collection and analyses were not blinded due to the complexity of the experiments. However, the use of software and machine-based analyses helped minimize potential investigator bias.

Reporting for specific materials, systems and methods

We require information from authors about some types of materials, experimental systems and methods used in many studies. Here, indicate whether each material, system or method listed is relevant to your study. If you are not sure if a list item applies to your research, read the appropriate section before selecting a response.

Materials & experimental systems

n/a	Involved in the study
☐	☒ Antibodies
☐	☒ Eukaryotic cell lines
☒	☐ Palaeontology and archaeology
☐	☒ Animals and other organisms
☒	☐ Clinical data
☒	☐ Dual use research of concern
☒	☐ Plants

Methods

n/a	Involved in the study
☒	☐ ChIP-seq
☐	☒ Flow cytometry
☒	☐ MRI-based neuroimaging

Antibodies

Antibodies used

TM6SF2 antibody (9E9, Prof. Helen Hobbs; #201AP, FabGennix, Frisco, TX); E-cadherin (RRID:AB_2728770, #14472, Cell Signaling Technology, Danvers, MA); Villin (NBP1-32841, Novus Biologicals, Littleton, CO); phospho-NF-κB p65 (Ser536) (RRID:AB_331284, #3033S, Cell Signalling Technology); NF-κB p65 (RRID: AB_10859369, #8242S, Cell Signalling Technology); IκBα (RRID: AB_390781, #4814, Cell Signalling Technology); Occludin (RRID:AB_2934013, #91131, Cell Signalling Technology); Claudin 3 (RRID:AB_2833313, AF0129, Affinity Biosciences); CD36 (RRID:AB_2716564, ab133625, Abcam, Cambridge, United Kingdom); NPC1L1 (RRID: AB_10976493, ab124801, Abcam); FABP5 (RRID:AB_2100341, 12348-1-AP, Proteintech, Wuhan, China); APC/Cyanine7 anti-mouse CD45 Recombinant Antibody (RRID:AB_2890720, Cat No. 157618, QA17A26, Biolegend, San Diego, CA), PE anti-mouse F4/80 Recombinant Antibody (RRID:AB_2832546, Cat No. 157303, QA17A29, Biolegend), PE/Cyanine7 anti-mouse/human CD11b Antibody (RRID:AB_312798, Cat. No. 101215, M1/70, Biolegend), PerCP/Cyanine5.5 anti-mouse CD206 (MMR) Antibody (RRID:AB_2561991, Cat. No. 141715, C068C2, Biolegend), APC anti-mouse CD11c antibodies (RRID:AB_313778, Cat. No. 117309, N418, Biolegend); FBD Horizon™ Fixable Viability Stain 520 (RRID:AB_2869573, Cat. No. 564407, BD Bioscience).

Validation

TM6SF2 antibody (FabGennix, #201AP) was validated in mouse liver tissues using IHC and WB. https://fabgennix.com/TM6SF2-Antibody
E-cadherin (Cell Signaling Technology, #14472) was validated in various cell lines by WB and IF. https://www.cellsignal.com/products/primary-antibodies/e-cadherin-4a2-mouse-mab/14472?srsltid=AfmBOorGUh37qRLyB3w-8DKi2uDWjP4n1iR-oK5E6PocTl842gW2D1Sj
Villin (Novus Biologicals, #NBP1-32841) was validated in cell extracts and colon tissues by WB and IF. https://www.novusbio.com/products/villin-1-antibody_nbp1-32841
phospho-NF-κB p65 (Ser536) (Cell Signalling Technology, #3033S) was validated in cell extracts by WB. https://www.cellsignal.com/products/primary-antibodies/phospho-nf-kb-p65-ser536-93h1-rabbit-mab/3033?srsltid=AfmBOoo_CPX3heKj7B5LOKcn7O7x0jlVFnDxENDGAmvUaKQLPp16uUIH
NF-κB p65 (Cell Signalling Technology, #8242S) was validated in various cell extracts by WB. https://www.cellsignal.com/products/primary-antibodies/nf-kb-p65-d14e12-xp-rabbit-mab/8242
IκBα (Cell Signalling Technology, #4814) was validated in various cell extracts by WB. https://www.cellsignal.com/products/primary-antibodies/ikba-l35a5-mouse-mab-amino-terminal-antigen/4814
Occludin (Cell Signalling Technology, #91131) was validated from DLD-1 cell extracts by WB. https://www.cellsignal.com/products/primary-antibodies/occludin-e6b4r-rabbit-mab/91131
Claudin 3 (Affinity Biosciences, AF0129) was validated from various cell extracts by WB. https://www.affbiotech.com/images/upload/File/affinity-wb-handbook-en.pdf
CD36 (Abcam, ab133625) was validated from various cell extracts by WB. https://www.abcam.com/en-hk/products/primary-antibodies/cd36-antibody-epr6573-ab133625#overlay=images&application=wb
NPC1L1 (Abcam, ab124801) was validated in HeLa whole cell lysate and human fetal liver tissues by WB. https://www.abcam.com/en-hk/products/primary-antibodies/niemann-pick-c1-like-1-npc1l1-antibody-epr5717-ab124801#application=wb
FABP5 (Proteintech, 12348-1-AP) was validated in A375 cells, HepG2 cells, mouse skin tissue, HeLa cells, A431 cells by WB. https://www.ptglab.com/products/FABP5-Antibody-12348-1-AP.htm
APC/Cyanine7 anti-mouse CD45 Recombinant Antibody (Biolegend, 157618) was validated in mouse splenocytes by flow cytometry. https://www.biolegend.com/ja-jp/products/apc-cyanine7-anti-mouse-cd45-recombinant-antibody-20633?GroupID=ImportedGROUP1
PE anti-mouse F4/80 Recombinant Antibody Biolegend, 157303) was validated in mouse peritoneal macrophages by flow cytometry. https://www.biolegend.com/en-ie/products/pe-anti-mouse-f4-80-recombinant-antibody-18755
PE/Cyanine7 anti-mouse/human CD11b Antibody (Biolegend, 101215) was validated in mouse bone marrow cells by flow cytometry. https://www.biolegend.com/ja-jp/products/pe-cyanine7-anti-mouse-human-cd11b-antibody-1921
PerCP/Cyanine5.5 anti-mouse CD206 (MMR) Antibody (Biolegend, 141715) was validated in Thioglycollate-elicited BALB/c mouse peritoneal macrophages by flow cytometry. https://www.biolegend.com/ja-jp/products/percp-cyanine5-5-anti-mouse-cd206-mmr-antibody-8477
APC anti-mouse CD11c antibodies (Biolegend, 117309) was validated in C57BL/6 mouse splenocytes by flow cytometry. https://www.biolegend.com/ja-jp/products/apc-anti-mouse-cd11c-antibody-1813
FBD Horizon™ Fixable Viability Stain 520 (BD Bioscience, 564407) was validated in human Jurkat cells by flow cytometry. https://www.bdbiosciences.com/en-eu/products/reagents/flow-cytometry-reagents/research-reagents/single-color-antibodies-ruo/fixable-viability-stain-520.564407.

Eukaryotic cell lines

Policy information about cell lines and Sex and Gender in Research

Cell line source(s)

AML-12, THLE-2, Caco2 and HEK293T cell lines were purchased from ATCC

Authentication	The authentication of AML-12, THLE-2, Caco2 and HEK293T cell lines was confirmed by Short Tandem Repeat Analysis (STR).
Mycoplasma contamination	These cell lines were tested negative for mycoplasma contamination.
Commonly misidentified lines (See ICLAC register)	None

Animals and other research organisms

Policy information about studies involving animals; ARRIVE guidelines recommended for reporting animal research, and Sex and Gender in Research

Laboratory animals	The conditional Tm6sf2 knockout mice at C57BL/6 background were generated through CRISPR-Cas9 system by Nanjing Biomedical Research Institute of Nanjing University, China. Tm6sf2flox mice were first generated by CRISPR-Cas9-targeted insertion of LoxP recombination sites into intronic regions that surround exons 2-5. The sgRNA sequences are: 5'-AGGGGAATCCACCTGTC; 3'-CCCAACACTCAACCCCCG. These Tm6sf2loxP mice (3-4 weeks) were then cross-bred with Cre transgenic mice by In vitro fertilization to yield Cre/Tm6sf2loxP mice. Tm6sf2 gene was inactivated due to the deletion of exons 2-5, induced by Cre-loxP recombination. Tissue specificity of conditional Tm6sf2 knockout was contingent upon tissue-specific expression of the Cre recombinase. Alb-Cre (B6.Cg-8 Tg (Alb-Cre) 21 Mgn/JNju mice, Nanjing University) or Villin-Cre mice (B6.Cg-Tg(Vil1-cre)997Gum/J mice, RRID:IMSR_JAX:004586, The Jackson Laboratory) were employed for liver-specific or IEC-specific Tm6sf2 knockout, respectively. Only homozygous conditional Tm6sf2 knockout mice were used for animal experiments. Systemic Tm6sf2 KO mice were generated at the Animal Centre of Xiamen University at C57BL/6 background using CRISPR/Cas9 technology. In brief, the CRISPR/Cas9-mediated gene editing led to a 4-base pair deletion in the first exon of the TM6SF2 gene, resulting in a frameshift mutation that effectively inactivated TM6SF2 (Extended Data Fig. 9B). This alteration was verified through Sanger sequencing. Backcross breeding with offsprings of C57BL/6 wildtype mice for 3 generations was used to remove any possible off-target changes. Another 2 batches of 7-week-old C57BL/6 mice were from the Laboratory Animal Services Centre of the Chinese University of Hong Kong. All SPF mice were housed in the animal center of Xiamen University and the Chinese University of Hong Kong on a 12-hour light/dark cycle and ad libitum assess to food and water. Mice were collectively housed in SPF conditions. Both male and female mice were used for some experiments according to the Sex and Gender Equity in Research (SAGER) guidelines. C57BL/6 male germ-free mice were bred at the Department of Laboratory Animal Services at the Army Medical University in Chongqing, China and Gnotobio Co Ltd, Dongguan, China.
Wild animals	No wild animals were used in this study.
Reporting on sex	Both male and female mice were used to investigate the role of intestinal Tm6sf2 deficiency in steatohepatitis. The results from male and female mice were consistent. For other experiments, male mice were used following the precedent set by prior MASLD studies that predominantly employed male mice.
Field-collected samples	No field collected samples were used in the study.
Ethics oversight	All animal studies were performed in accordance with guidelines approved by the Animal Experimentation Ethics Committee of Xiamen University, Army Medical University, Gnotobio and the Chinese University of Hong Kong

Note that full information on the approval of the study protocol must also be provided in the manuscript.

Flow Cytometry

Plots

Confirm that:

☒ The axis labels state the marker and fluorochrome used (e.g. CD4-FITC).

☒ The axis scales are clearly visible. Include numbers along axes only for bottom left plot of group (a 'group' is an analysis of identical markers).

☒ All plots are contour plots with outliers or pseudocolor plots.

☒ A numerical value for number of cells or percentage (with statistics) is provided.

Methodology

Sample preparation	Freshly isolated hepatic tissue was gently chopped in warm HBSS containing collagenase IV and incubated at 37 ℃ for 15 min. Ice-cold HBSS was added immediately to stop the action of the enzymes. The tissue suspension was filtered with 70 µm cell strainer, washed with PBS and centrifuged at 500 g for 10 min. 8 ml of resuspended cells was then added to 4ml of 80% Percoll. Cells were centrifuged at 500 g for 10min and resuspend immediately in FACS buffer.
Instrument	BD FACSCelestaTM flow cytometry (Biosciences, San Jose, CA)
Software	FlowJo software version 10 (Treestar Inc., San Carlos, CA)

Cell population abundance	The abundance of each cell population was provided in the figures. Purity was determined by flow cytometry and confirmed in our data analysis.
Gating strategy	Initially, all events were detected using FSC-A/SSC-A gating. Subsequently, CD45/APC-cy7 gating was implemented to isolate CD45+ cells. The selection of single cells was achieved through FSC-A/FSC-H gating. Live cells were then distinguished using FITC-Fvc gating. Finally, F4/80+CD11b+ macrophages were identified using PE/F4/80 and PE-Cy7-CD11b gating, while M1 and M2 macrophages were discriminated based on APC/CD11c and PerCP-cy5.5/CD206 gating, respectively.

☒ Tick this box to confirm that a figure exemplifying the gating strategy is provided in the Supplementary Information.